A single tyrosine phosphorylation site in cortactin is important for filopodia formation in neuronal growth cones

Yuan Ren[a,†], Yingpei He[a], Sherlene Brown[b], Erica Zbornik[a], Michael J. Mlodzianoski[c,‡], Donghan Ma[c], Fang Huang[c,d,e], Seema Mattoo[a,d], and Daniel M. Suter[a,e,f,g,*]

Departments of [a]Biological Sciences and [b]Biochemistry, [c]Weldon School of Biomedical Engineering, Purdue Institutes of [d]Inflammation, Immunology and Infectious Disease and [e]Integrative Neuroscience, [f]Bindley Bioscience Center, and [g]Birck Nanotechnology Center, Purdue University, West Lafayette, IN 47907

ABSTRACT **Cortactin is a Src tyrosine phosphorylation substrate that regulates multiple actin-related cellular processes. While frequently studied in nonneuronal cells, the functions of cortactin in neuronal growth cones are not well understood. We recently reported that cortactin mediates the effects of Src tyrosine kinase in regulating actin organization and dynamics in both lamellipodia and filopodia of *Aplysia* growth cones. Here, we identified a single cortactin tyrosine phosphorylation site (Y499) to be important for the formation of filopodia. Overexpression of a 499F phospho-deficient cortactin mutant decreased filopodia length and density, whereas overexpression of a 499E phospho-mimetic mutant increased filopodia length. Using an antibody against cortactin pY499, we showed that tyrosine-phosphorylated cortactin is enriched along the leading edge. The leading edge localization of phosphorylated cortactin is Src2-dependent, F-actin–independent, and important for filopodia formation. In vitro kinase assays revealed that Src2 phosphorylates cortactin at Y499, although Y505 is the preferred site in vitro. Finally, we provide evidence that Arp2/3 complex acts downstream of phosphorylated cortactin to regulate density but not length of filopodia. In conclusion, we have characterized a tyrosine phosphorylation site in *Aplysia* cortactin that plays a major role in the Src/cortactin/Arp2/3 signaling pathway controlling filopodia formation.**

Monitoring Editor
Paul Forscher
Yale University

Received: Apr 2, 2018
Revised: May 1, 2019
Accepted: May 16, 2019

INTRODUCTION

Proper wiring of neurons is key to the functionality of the nervous system. This is achieved by a specialized extension referred to as the neuronal growth cone located at the tips of axons and dendrites during both development and regeneration (Lowery and Van Vactor, 2009; Vitriol and Zheng, 2012). As a sensory unit, the neuronal growth cone is equipped with an exquisite molecular machinery to make decisions about growth rate and direction in response to a multitude of environmental cues (Davenport *et al.*, 1993; Suter and Forscher, 2000; Dickson, 2002). As a motile structure, these extracellular biochemical or biophysical cues are translated into intracellular signals to constantly guide the remodeling of its actin and microtubule cytoskeleton, the major force generators and mediators of growth cone motility (Dent *et al.*, 2011; Suter and Miller, 2011; Gomez and Letourneau, 2014; Athamneh and Suter, 2015; Omotade *et al.*, 2017). Therefore, investigations into the regulation of actin organization and dynamics in the context of growth cone motility are instrumental for our understanding of development and regeneration of nervous system. However, the detailed picture of signaling pathways that relay information from membrane receptors to the underlying actin cytoskeleton is still incomplete, thwarting efforts to further our knowledge about neurite regeneration.

Filopodia are F-actin–rich, fingerlike exploratory protrusions that can emerge from many different cell types including neurons

This article was published online ahead of print in MBoC in Press (http://www.molbiolcell.org/cgi/doi/10.1091/mbc.E18-04-0202) on May 22, 2019.

Present addresses: [†]Department of Molecular Biophysics & Biochemistry, Yale University, New Haven, CT 06516; [‡]Centre for Dynamic Imaging, The Walter and Eliza Hall Institute for Medical Research, Parkville, VIC 3052, Australia.

*Address correspondence to: Daniel Suter (dsuter@purdue.edu).

Abbreviations used ASW, artificial sea water; BME, β-mercaptoethanol; BSA, bovine serum albumin; DIC, differential interference contrast; DMSO, dimethyl sulfoxide; DNSrc2, dominant negative Src2; dSTORM, Direct Stochastic Optical Reconstruction Microscopy; FBS, fetal bovine serum; FFF mutant, triple tyrosine phosphorylation cortactin mutant; LIS-ASW, low ionic strength artificial sea water; NTA, N-terminal acidic; P, peripheral; PBS, phosphate-buffered saline; SEC, size exclusion chromatography; WT, wild type.

(Gallo, 2013). They are highly dynamic structures that develop from multiple locations on the neuronal surface including the cell body, axon, dendrites, as well as the growth cone. Filopodia serve multiple functions during neuronal development including initiation of axons and dendrites (Smith, 1994; Dent *et al.*, 2007), axonal guidance (O'Connor and Bentley, 1993; Gomez and Letourneau, 1994; Gallo *et al.*, 1997), formation of axonal and dendritic branches (Spillane *et al.*, 2011), as well as of synapses (Ozcan, 2017). They are made up by bundles of highly oriented F-actin filaments (Lewis and Bridgman, 1992) and are wrapped by the plasma membrane to form slender devices that can detect changes in extracellular signals (Davenport *et al.*, 1993; Gomez and Letourneau, 1994; Gallo *et al.*, 1997; Gallo, 2013; McConnell *et al.*, 2016), guide extension of microtubules (Schaefer *et al.*, 2002; Burnette *et al.*, 2007), and apply traction force to substrates (Heidemann *et al.*, 1990; Chan and Odde, 2008). In the growth cone peripheral (P)-domain, filopodia are usually embedded within a meshwork of cross-linked F-actin or lamellipodia (Lewis and Bridgman, 1992), with which they share some of the same signaling and regulatory machineries (Small *et al.*, 2002; Faix and Rottner, 2006; Korobova and Svitkina, 2008; Gallo, 2013; He *et al.*, 2015). Whereas it is generally agreed that filopodia formation requires coordinated elongation of unipolar actin filaments, different molecular mechanisms have been proposed with respect to the initiation of filopodia formation (Svitkina *et al.*, 2003; Faix and Rottner, 2006; Block *et al.*, 2008; Korobova and Svitkina, 2008; Norris *et al.*, 2009; Goncalves-Pimentel *et al.*, 2011). Their dynamic behavior depends on the rates of actin assembly at the filopodia tip, as well as myosin-driven retrograde flow and actin recycling at the base of the filopodial bundle (Lin *et al.*, 1996; Mallavarapu and Mitchison, 1999).

Initially characterized as a substrate for Src kinase, cortactin was soon found to be a key player in many actin-related processes, including cell migration, endocytosis, cell–cell connection, tumor invasion, and pathogen response (Wu and Parsons, 1993; Weed and Parsons, 2001; Cosen-Binker and Kapus, 2006; MacGrath and Koleske, 2012; Schnoor *et al.*, 2018). A major portion of cortactin's effect on actin remodeling is attributed to its ability to activate Arp2/3 complex through its N-terminal acidic (NTA) domain, to its F-actin–binding via tandem repeats, and through its interaction with other nucleation promoting factors such as N-WASP via its C-terminal SH3 domain (Weed *et al.*, 2000; Uruno *et al.*, 2001; Weaver *et al.*, 2001; Weed and Parsons, 2001; Schnoor *et al.*, 2018). Consequently, cortactin is important in the assembly, branching, and stabilization of actin-based cytoskeletal structures such as lamellipodia, invadopodia, and filopodia (Bryce *et al.*, 2005; Desmarais *et al.*, 2009; Siton *et al.*, 2011; Helgeson and Nolen, 2013; He *et al.*, 2015). Moreover, the function of cortactin is subject to multiple posttranslational modifications, including phosphorylation, acetylation, and ubiquitination; however, the functional consequences of these modifications with respect to actin remodeling are still under debate, especially with respect to the role of tyrosine phosphorylation in actin assembly (Martinez-Quiles *et al.*, 2004; Zhang *et al.*, 2007; Ayala *et al.*, 2008; Oser *et al.*, 2010; Schnoor *et al.*, 2018). In neuronal growth cones, cortactin has been implicated in the formation and stabilization of filopodia, in lamellipodia protrusion, and consequently neuronal growth cone motility (Kurklinsky *et al.*, 2011; Yamada *et al.*, 2013; He *et al.*, 2015; Kubo *et al.*, 2015).

Not much is known about the role of Src-mediated tyrosine phosphorylation in the formation of filopodia. By taking advantage of the large growth cones elaborated by cultured *Aplysia* bag cell neurons, we have recently shown how Src and cortactin cooperate to regulate actin organization and dynamics in neuronal growth cones and uncovered an important role of cortactin in filopodia formation and maintenance (He *et al.*, 2015). Here, we identified a single tyrosine residue, Y499, in *Aplysia* cortactin as the critical Src phosphorylation site for promoting filopodia formation in growth cones. Using a phospho-specific cortactin antibody, we located tyrosine-phosphorylated cortactin at the leading edge of growth cones and provided evidence that *Aplysia* Src2 can phosphorylate cortactin in cultured neurons. We also provide the first direct biochemical evidence that *Aplysia* Src2 phosphorylates *Aplysia* cortactin. Furthermore, we discovered an F-actin–independent anchoring of tyrosine-phosphorylated cortactin at the growth cone leading edge, and we showed that this localization of phosphorylated cortactin is crucial for filopodia formation. Last, by inhibiting both the Arp2/3 complex and cortactin phosphorylation, we showed that phosphorylated cortactin acts upstream of Arp2/3 complex to regulate filopodia density most likely by initiation of filopodia but not the length of filopodia. In conclusion, our results delineate an important Src2-cortactin-Arp2/3-actin pathway with the potential of relaying extracellular signals to intracellular remodeling of actin cytoskeleton, such as formation of filopodia.

RESULTS

The phosphorylation state of Y499 in *Aplysia* cortactin is important for filopodia formation

We have recently shown that overexpression of an *Aplysia* cortactin mutant that cannot be phosphorylated at any of the three putative tyrosine phosphorylation sites Y499, Y505, and Y509 (FFF mutant) decreased both filopodia length and density in growth cones (He *et al.*, 2015). These findings suggested that tyrosine phosphorylation of cortactin is critical for filopodia formation and stability. Since none of these three tyrosine residues clearly align with any of the known tyrosine phosphorylation sites in mouse cortactin, Y421, Y466, and Y482, we created single tyrosine phosphorylation mutants of *Aplysia* cortactin in order to identify the tyrosine residue that is critical for the filopodia phenotypes mentioned above. We then expressed these individual tyrosine cortactin mutants in cultured *Aplysia* bag cell neurons and analyzed filopodia phenotypes in order to determine the single phosphorylation-defective cortactin mutant(s) that phenocopies the cortactin FFF mutant. Therefore, we analyzed filopodial density and length of growth cones following overexpression of single tyrosine phosphorylation-defective cortactin mutants, FFF cortactin mutant, or wild-type (WT) cortactin in cultured *Aplysia* bag cell neurons (Figure 1). The leading edge in the P-domain of a growth cone (boxed region in Figure 1A) from each experimental group is shown in both differential interference contrast (DIC) (Figure 1, B–H) and fluorescent channel revealing total cortactin protein following immunostaining (Figure 1, B′–H′). Among all three single tyrosine mutants, only 499F overexpression faithfully recapitulated the reduced filopodial density and length phenotype caused by the FFF mutant when compared with uninjected or dextran injection controls (Figure 1). WT cortactin overexpression increased filopodial length but not density compared with controls (Figure 1, J–K). In summary, these results suggest that Y499 is the critical tyrosine phosphorylation residue in *Aplysia* cortactin with respect to filopodia formation.

As a complementary approach, we mutated the Y499 site to glutamic acid, thereby creating a phospho-mimetic 499E mutant. After overexpression of either the 499E or the EEE (triple phosphomimetic mutant), filopodial density was not significantly changed when compared with control conditions (Figure 2, A–D, A′–D′, and I), similar to the overexpression of WT cortactin (Figure 1J). On the other hand, overexpression of either the 499E or the EEE cortactin

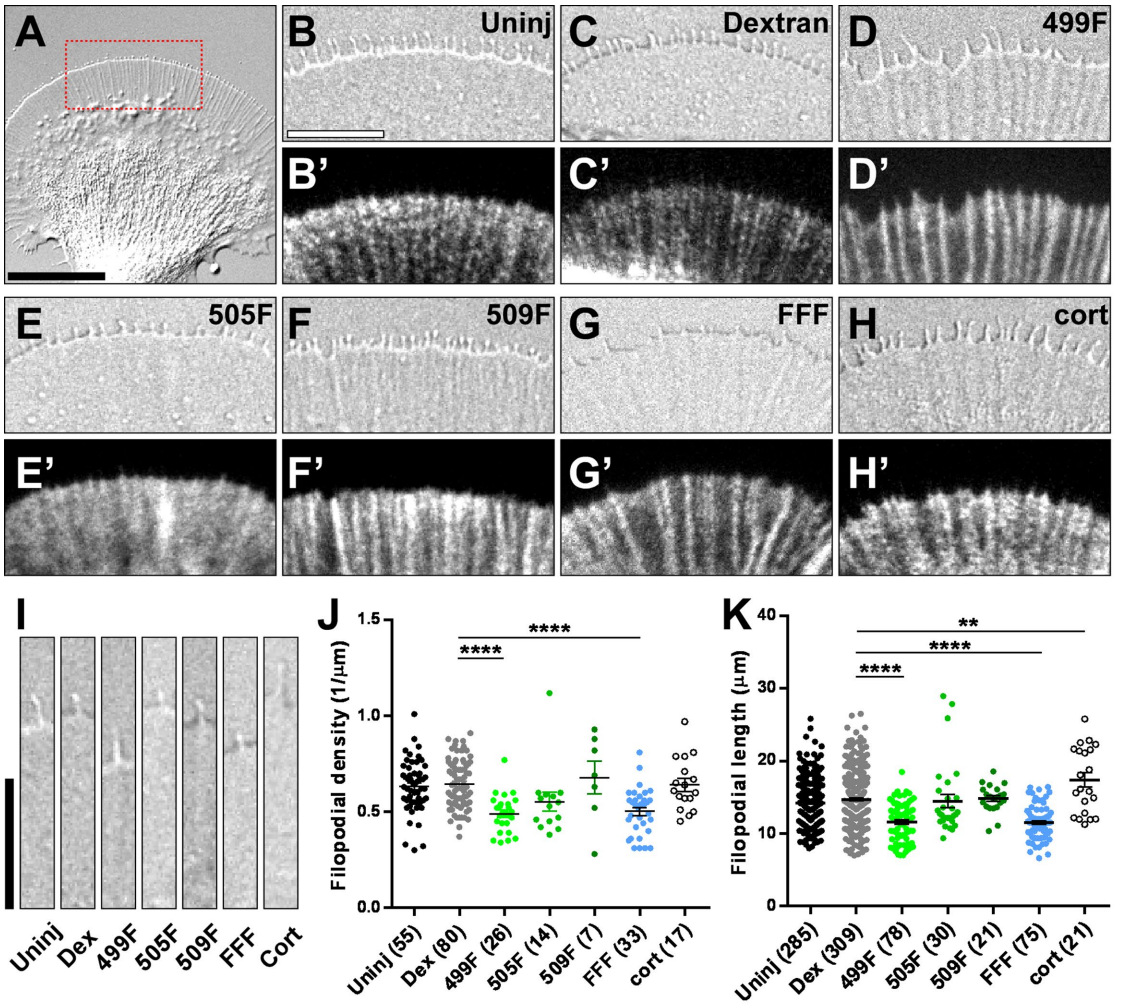

FIGURE 1: Growth cone filopodial density and length are reduced by overexpression of cortactin 499F mutant. (A) DIC image of an *Aplysia* growth cone. Filopodia organization in the boxed region is quantified. (B–H) DIC images of filopodia at the growth cone leading edge. (B'–H') Immunostaining of total cortactin with 4F11 antibody. Overexpressed cortactin localized along filopodia. (I) A filopodium from each group was selected for length comparison. The bottom of the image corresponds to the filopodium base. (J) Expression of 499F and FFF cortactin mutants but not WT cortactin significantly reduced filopodial density when compared with uninjected (Uninj) and dextran (Dex) injection controls. Numbers in parentheses indicate numbers of growth cones analyzed. (K) 499F and FFF cortactin mutants significantly reduced filopodial length, while overexpression of WT cortactin increased filopodial length. Numbers in parentheses are numbers of filopodia analyzed. Data are presented as mean ± SEM and pooled from six independent experiments. $^{**}P < 0.01$. $^{****}P < 0.0001$. Analysis of variance (ANOVA) with Dunnett's multiple comparison. Scale bar in A: 20 μm; B: 10 μm; I: 10 μm.

mutants increased filopodial length (Figure 2, A–D, A'-D', and J) similar to what we observed when expressing WT cortactin (Figure 1K). This indicates that the 499E mutant causes a similar filopodia length phenotype as the triple phospho-mimetic mutant EEE, again, suggesting that the Y499 is the critical tyrosine phosphorylation site with respect to filopodia length regulation. To further confirm that Y499 is the only critical phosphorylation site controlling filopodial density and length, two more cortactin mutants were generated. In the FEE mutant, the Y499 site was mutated to phenylalanine and the Y505 and Y509 sites to glutamic acid. Similarly, in the EFF mutant, the Y499 was mutated to glutamic acid and the Y505 and Y509 sites to phenylalanine. As shown in Figure 2, G, G', K, and L, overexpression of the FEE mutant decreased filopodial density and filopodial length phenocopying the FFF mutant (Figure 1, J and K). Overexpression of the EFF mutant led to increased filopodial length without further increasing filopodial density (Figure 2, H, H', K, and L), which is similar to the phenotype induced by overexpression of EEE. Altogether, these cell biological results indicate that Y499 is the only critical tyrosine residue in *Aplysia* cortactin that mediates the function of phosphorylated cortactin with respect to filopodia formation and length regulation.

Tyrosine-phosphorylated cortactin is enriched at the growth cone leading edge

To further investigate the function of cortactin tyrosine phosphorylation at Y499, we made a polyclonal phospho-specific peptide antibody against cortactin-pY499 (p-cort; cortactin 493–504: PERVEDpYGEETE) and one against the same nonphosphorylated peptide (n-cort; PERVEDYGEETE). First, we verified the specificity of both antibodies by Western blotting of *Aplysia* CNS lysate and purified bacterially expressed *Aplysia* cortactin protein (Supplemental Figure S1). Native vertebrate cortactin commonly runs as a p80/85

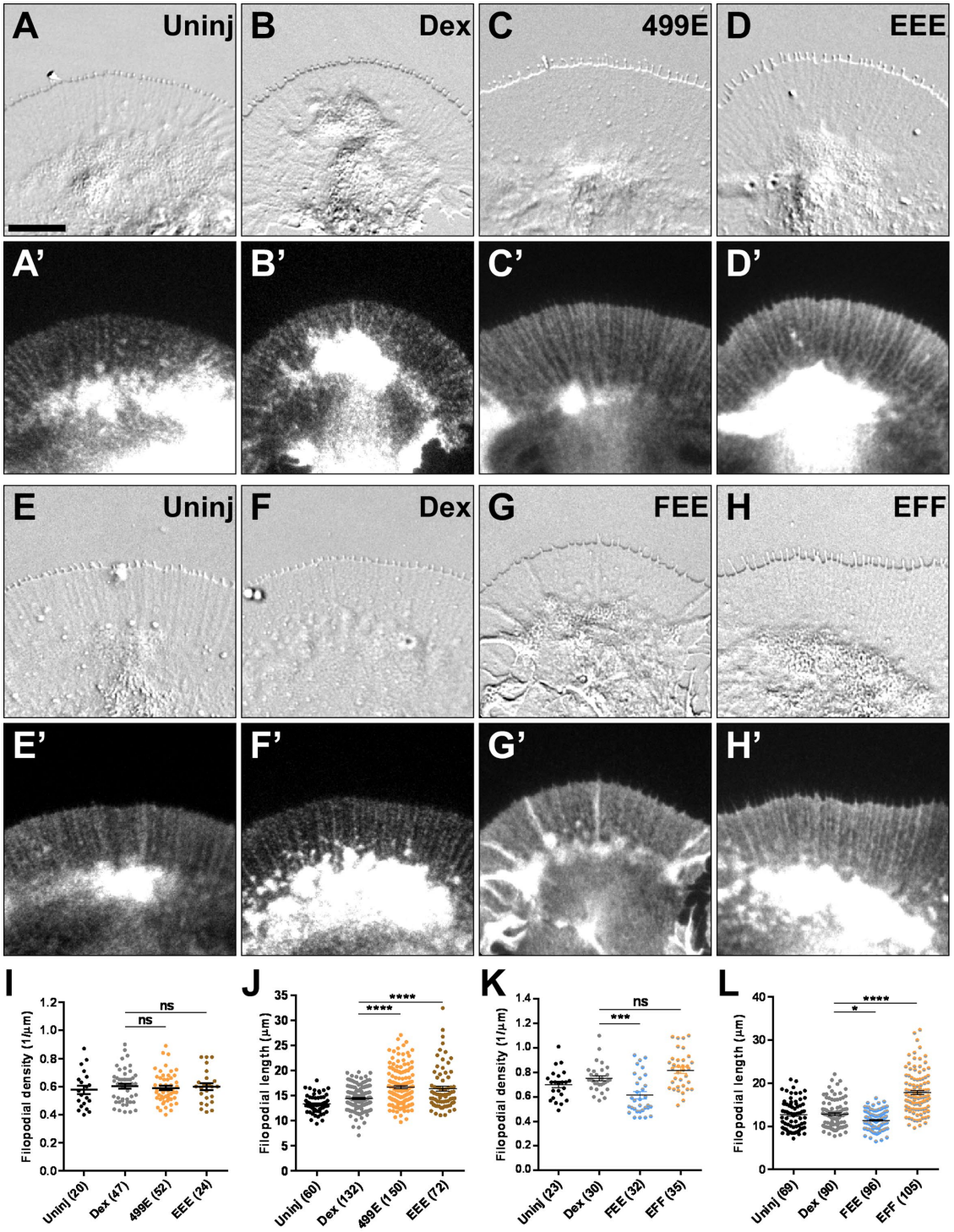

FIGURE 2: Cortactin Y499 is the only phosphorylation site relevant for regulating filopodia formation. (A–H) DIC images of growth cones with injection of different mutant cortactin mRNAs. (A'–H') Immunostaining of total cortactin with 4F11 antibody. (I) Filopodial density was not altered after either 499E or EEE cortactin mutant overexpression when compared with uninjected (Uninj) or dextran (Dex)-injected control neurons. Numbers in parenthesis are numbers of growth cones analyzed. (J) Filopodial length is increased by expressing either the phospho-mimetic 499E or the EEE cortactin mutant when compared with controls. Data are presented as mean ± SEM and are representative of two independent experiments. Numbers in parenthesis are numbers of filopodia analyzed. ****$P < 0.0001$. Dunnett's multiple comparison. (K) FEE mutant significantly decreased filopodia density compared with controls. Numbers in parenthesis are numbers of growth cones analyzed. (L) EFF mutant significantly increased filopodial length, while FEE significantly decreased filopodia length. This suggests that the phosphorylation state of cortactin Y499 dictates the function of cortactin in filopodia length and formation. Data are presented as mean ± SEM and are representative of two independent experiments. Numbers in parenthesis are numbers of filopodia analyzed. *$P < 0.05$. ***$P < 0.001$. ****$P < 0.0001$. ANOVA with Dunnett's multiple comparison. Scale bar: 10 µm.

doublet on SDS–PAGE, where the mobility shift of between the two bands was proposed to result from posttranslational modifications and/or conformational changes (Wu and Parsons, 1993; Huang *et al.*, 1997; van Damme *et al.*, 1997; Ammer and Weed, 2008). *Aplysia* cortactin runs at a slightly higher molecular weight as a 95/110 kDa doublet (Supplemental Figure S1) (Decourt *et al.*, 2009). The p-cort antibody recognized both bands in *Aplysia* CNS lysates (Supplemental Figure S1, A and B), whereas the n-cort antibody only detected the lower band (Supplemental Figure S1C). The intensity of the upper band detected by the p-cort antibody could be reduced by Src kinase inhibition with PP2 (Supplemental Figure S1A), and both bands could be completely blocked after adding the cognate p-cort peptide to the primary antibody solution (Supplemental Figure S1B). Both p-cort and n-cort antibodies also recognized purified bacterially expressed *Aplysia* cortactin, which suggests that both conformations of cortactin contain both phosphorylation states (Supplemental Figure S1D). Inclusion of either p-cort or n-cort peptides for respective antibodies during immunostaining of growth cone greatly reduced fluorescence intensity in their corresponding channel, without affecting the staining pattern of either total cortactin or actin (Supplemental Figure S2, compare the signal intensity between C and G and between O and S). Taken together, we have obtained two reliable antibodies that can be used to probe the phosphorylation state of *Aplysia* cortactin.

In control growth cones, p-cort staining showed a striking preferential localization of tyrosine-phosphorylated cortactin along the leading edge of growth cones, quite different from the pattern of total cortactin as detected by the monoclonal antibody 4F11, which was relatively more homogeneous in P-domain, enriched along filopodia shafts, and generally reflecting F-actin distribution (Figures 3, A–C, 1, B′–H′, and 2, A′–H′) (Decourt *et al.*, 2009). By calculating the ratiometric value of phosphorylated over total cortactin for each pixel, we found that the leading edge exhibits the highest level of cortactin phosphorylation in the growth cones (Figure 3D). The preferential localization of the p-cortactin signal along the leading edge mirrors the localization of activated pSrc2 (Wu *et al.*, 2008; He *et al.*, 2015) and can be effectively removed when growth cones are treated with 25 µM Src inhibitor PP2 for 15 min (Figure 3, E–H). This significant reduction in p-cort signal was due to reduced phosphorylation, since the amount of total cortactin remained constant (Figure 3, E–K). To acquire more detailed information on the localization of phosphorylated cortactin, we performed superresolution imaging via direct Stochastic Optical Reconstruction Microscopy (dSTORM) and p-cort antibody labeling (Figure 3, L and M). We confirmed the localization of phosphorylated cortactin along growth cone leading edge and at the filopodia tips. Importantly, we detected an abrupt drop of phosphorylated cortactin 200 nm into lamellipodia and no repetitive pattern along filopodia shafts, suggesting a tight spatial regulation of cortactin phosphorylation (Figure 3M). In conclusion, cortactin phosphorylated by Src is highly enriched along the leading edge and filopodia tips of neuronal growth cones depicting a similar distribution as activated Src2 (Wu *et al.*, 2008; He *et al.*, 2015).

Src2 phosphorylates cortactin at Y499 in growth cones

Aplysia express two Src tyrosine kinases referred to as Src1 and Src2 (Wu *et al.*, 2008). By overexpressing different Src2 and cortactin constructs in cultured neurons, we have recently provided functional evidence that Src2 phosphorylates cortactin and thereby controls filopodia formation and lamellipodia protrusion via the actin cytoskeleton (He *et al.*, 2015). Here, we went on to determine whether *Aplysia* Src2 phosphorylates cortactin at the Y499 site in neuronal growth cones. The cortactin phosphorylation ratio in the growth cone P-domain was compared between control cells injected with buffer only (CTRL) or Src2 mRNA (Src2) (Figure 4). Overexpression of Src2 led to a modest but significant increase of cortactin phosphorylation (Figure 4Q), without changing the preferential localization of phosphorylated cortactin along growth cone leading edge and near filopodia tips (Figure 4, G and H). These results confirm that cortactin indeed is phosphorylated by Src2 at Y499 in growth cones. To further validate our p-cort antibody, we overexpressed either WT cortactin or the triple tyrosine phosphorylation-defective mutant FFF (Figure 4, I–P). As expected, only overexpression of WT cortactin led to an increase of the p-cort signal (Figure 4R). Interestingly, overexpression not only of the FFF mutant but also of WT cortactin resulted in a reduction of cortactin phosphorylation ratio when compared with controls (Figure 4T).

Recombinant *Aplysia* Src2 phosphorylates *Aplysia* cortactin in vitro

We previously showed a partial colocalization of Src2 and cortactin in *Aplysia* bag cell neuronal growth cones and demonstrated that both Src2 and cortactin have a critical role in the formation and stability of filopodia and lamellipodia (He *et al.*, 2015). Here, we provided evidence that Src2 phosphorylates Y499 of cortactin in cultured neurons (Figure 4). To determine whether *Aplysia* Src2 directly phosphorylates *Aplysia* cortactin and whether Y499 is the preferred site of phosphorylation, we performed an in vitro kinase assay where recombinant WT cortactin or individual cortactin tyrosine phosphorylation site mutants (YFF, FYF, FFY, or FFF) were incubated with recombinant active WT Src2 kinase or enzymatically inactive dominant negative Src2 (DNSrc2) kinase using γ-^{32}P-ATP as a nucleotide source. DNSrc2 is a dominant negative form of Src2, which is a kinase-dead mutant in the open conformation (K286M Y518F) (He *et al.*, 2015). To ensure bacterially expressed and purified recombinant *Aplysia* cortactin was not prephosphorylated by bacterial proteins, cortactin was initially copurified with a phosphatase (YopH) and further purified by size exclusion chromatography (SEC). The SEC profile and corresponding cortactin-associated peak analyzed by Coomassie gel are shown in Figure 5, A and B. WT cortactin and its tyrosine phosphorylation mutants eluted as a single predominant peak at an elution volume corresponding to 55 ml, indicating that all proteins purified and folded with a similar conformation (Figure 5A). Smaller SEC peaks at 85 and 130 ml represent low molecular weight contaminants and void volume, respectively. WT cortactin also showed a second small peak at 45 ml, which may represent potentially oligomeric forms. Therefore, to ensure we analyzed WT cortactin and all its mutants that displayed similar biochemical properties, we conducted our experiments with samples corresponding to the 55-ml peak. SDS–PAGE and Coomassie analysis of cortactin samples corresponding to this 55-ml peak showed a similar migration pattern with the WT protein and mutants appearing as a doublet with a lower band at 95 kDa and an upper band at ~110 kDa (Figure 5B).

Next, the above SEC-purified, unphosphorylated cortactin proteins were evaluated for phosphorylation by purified active WT Src2 or inactive DNSrc2 in an in vitro kinase assay and assessed by autoradiography of the SDS–PAGE gel. As expected, a representative autoradiograph shows that Src2 was active as determined by its ability to autophosphorylate (Figure 5C; ~65 kDa band), while DNSrc2 did not display any radioactive band on the autoradiograph. Furthermore only WT Src2 phosphorylated all cortactin samples to varying degrees (left gel), while no signal was detected for samples treated with DNSrc2 (right gel). The lack of any radioactive signal associated with cortactin in the absence of Src2 also serves as a

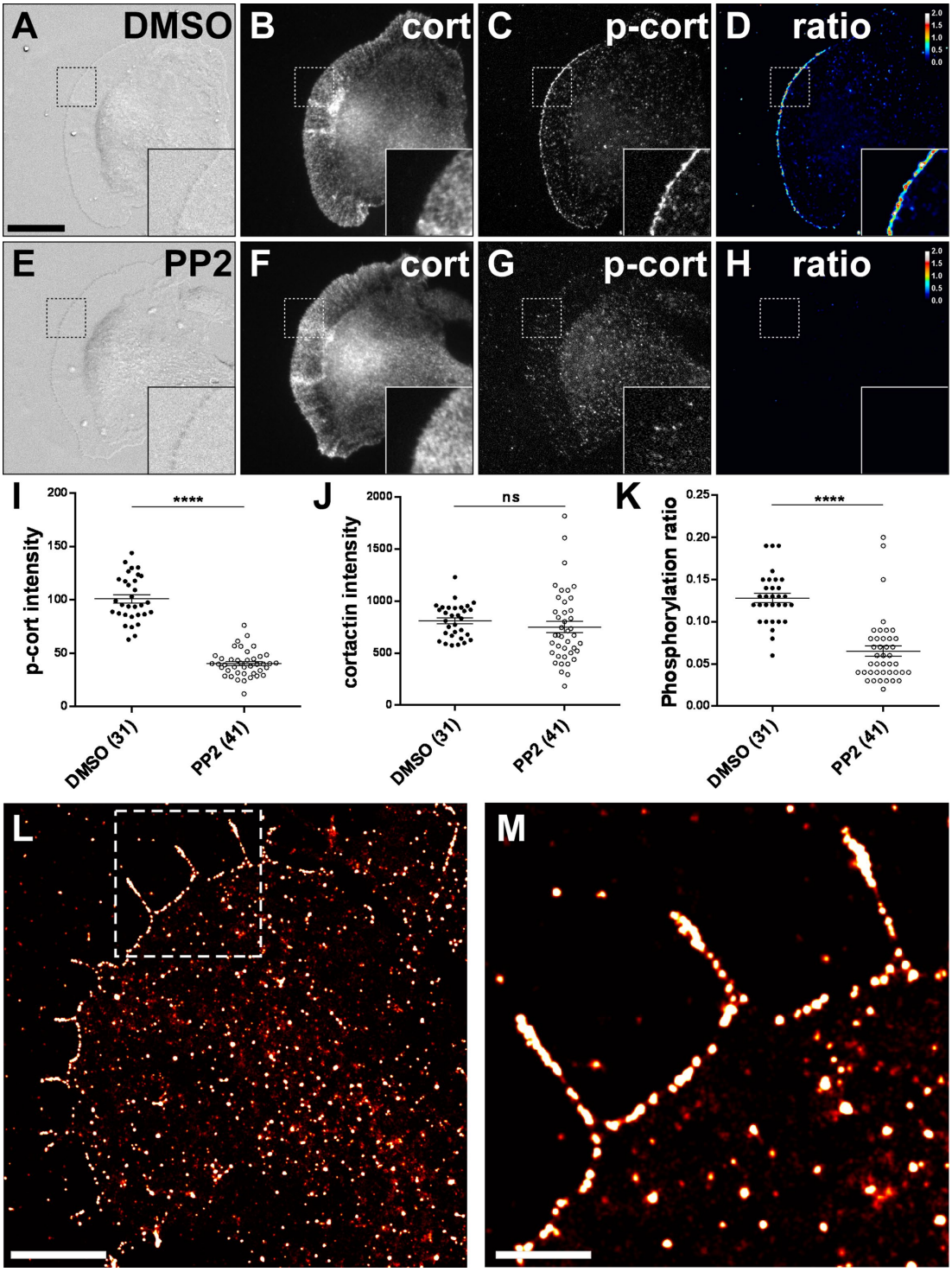

FIGURE 3: Phosphorylated cortactin is enriched at the growth cone leading edge. (A–D) Images of growth cones treated with 0.1% DMSO. (E–H) Images of growth cones treated with 25 μM Src2 inhibitor PP2 for 15 min. Immunostaining with both p-cortactin antibody and total cortactin antibody (4F11) was used to determine the level of cortactin phosphorylation. (A, E) DIC image; (B, F) immunostaining of total cortactin; (C, G) immunostaining of phosphorylated cortactin. (D, H) Cortactin phosphorylation ratio (background corrected p-cortactin/total cortactin) represented as a ratiometric image. Enlargements of boxed regions are shown as insets. PP2 treatment removed p-cortactin signals from the leading edge. (I–K) Quantification of p-cortactin intensity, total cortactin intensity, and cortactin phosphorylation ratio. PP2 treatment reduced p-cortactin ratio without affecting total cortactin level. Data are presented as mean ± SEM and are representative of four independent experiments. Numbers in parenthesis are numbers of growth cones analyzed. ****$P < 0.0001$. Unpaired *t* test. Scale bar: 20 μm. (L) dSTORM image of *Aplysia* growth cone stained with p-cort antibody. Phosphorylated cortactin signal was sporadic within P and C domain but concentrated along the leading edge and filopodia. (M) Magnified image of boxed region in L. Phosphorylated cortactin is enriched along leading edge and filopodia tip. Scale bar in L: 5 μm; M: 1 μm.

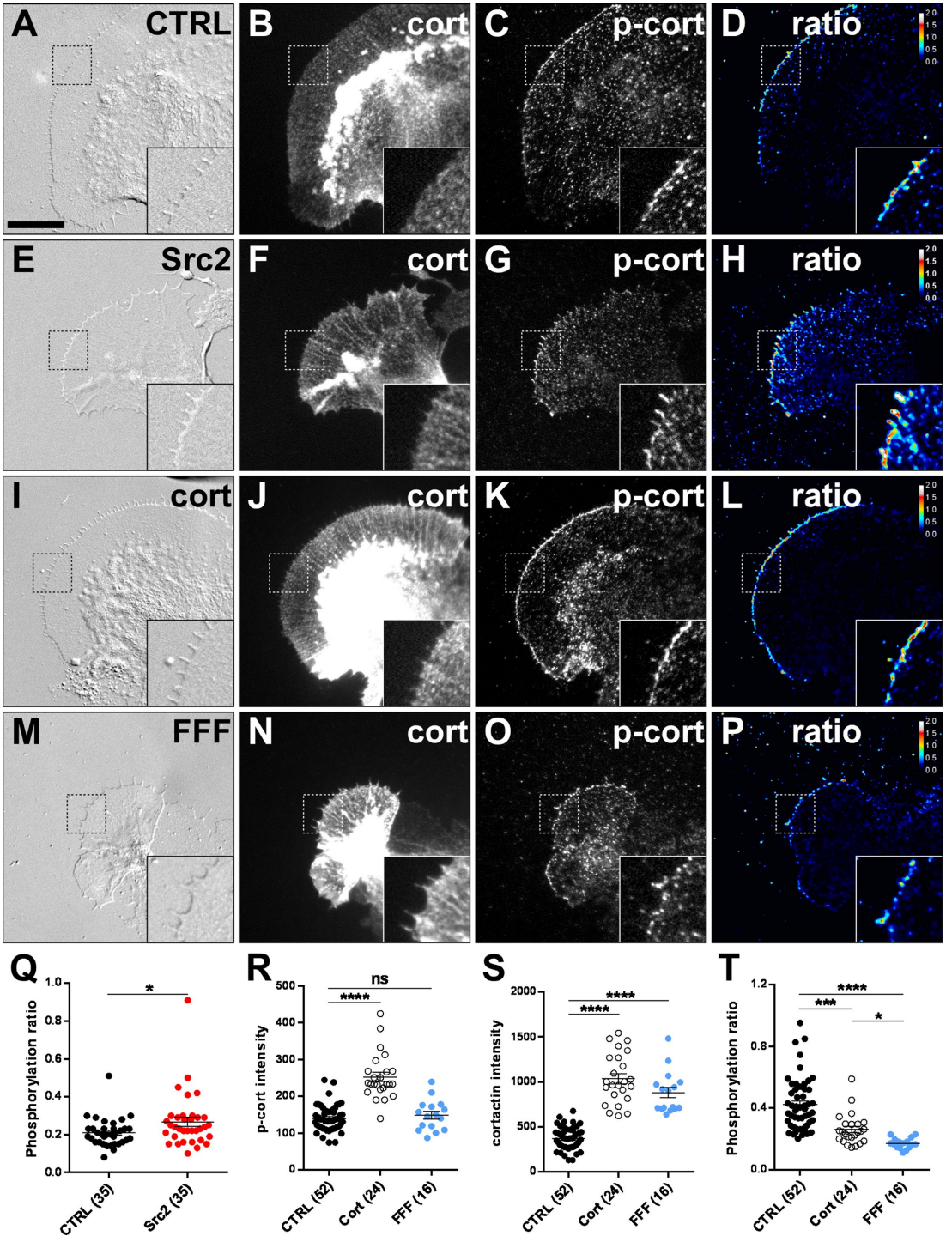

FIGURE 4: Src2 phosphorylates cortactin at Y499 in *Aplysia* neurons. (A–D) Images of a growth cone from neuron injected with buffer only (CTRL). (E–H) Images of growth cone that overexpresses Src2. (I–L) Images of growth cone that overexpresses WT cortactin. (M–P) Images of growth cone that overexpresses cortactin FFF. Immunostaining with both p-cortactin antibody and total cortactin antibody (4F11) was used to determine the level of cortactin phosphorylation. (A, E, I, M) DIC image; (B, F, J, N) immunostaining of total cortactin; (C, G, K, O) immunostaining of phosphorylated cortactin. (D, H, L, P) Cortactin phosphorylation ratio (background corrected p-cortactin/total cortactin) represented as a ratiometric image. Enlargements of boxed regions are shown as insets. Phosphorylated cortactin was found to be enriched at the leading edge and filopodial tips in all cases, regardless of overexpressed cortactin species. (Q) Cortactin phosphorylation ratio is significantly increased by Src2 overexpression when compared with control cells that were injected with buffer only. (R–T) Overexpression of WT cortactin led to increased cortactin phosphorylation level, whereas overexpression of cortactin FFF mutant did not. Overexpression of both WT cortactin and FFF reduced p-cortactin ratio. Data are presented as mean ± SEM and are representative of three independent experiments. Numbers in parenthesis are numbers of growth cones analyzed. *$P < 0.05$; ***$P < 0.001$, ****$P < 0.0001$. Unpaired *t* test for Q; ANOVA with Dunnett's multiple comparison for R, S, and T. Scale bar in A: 20 μm.

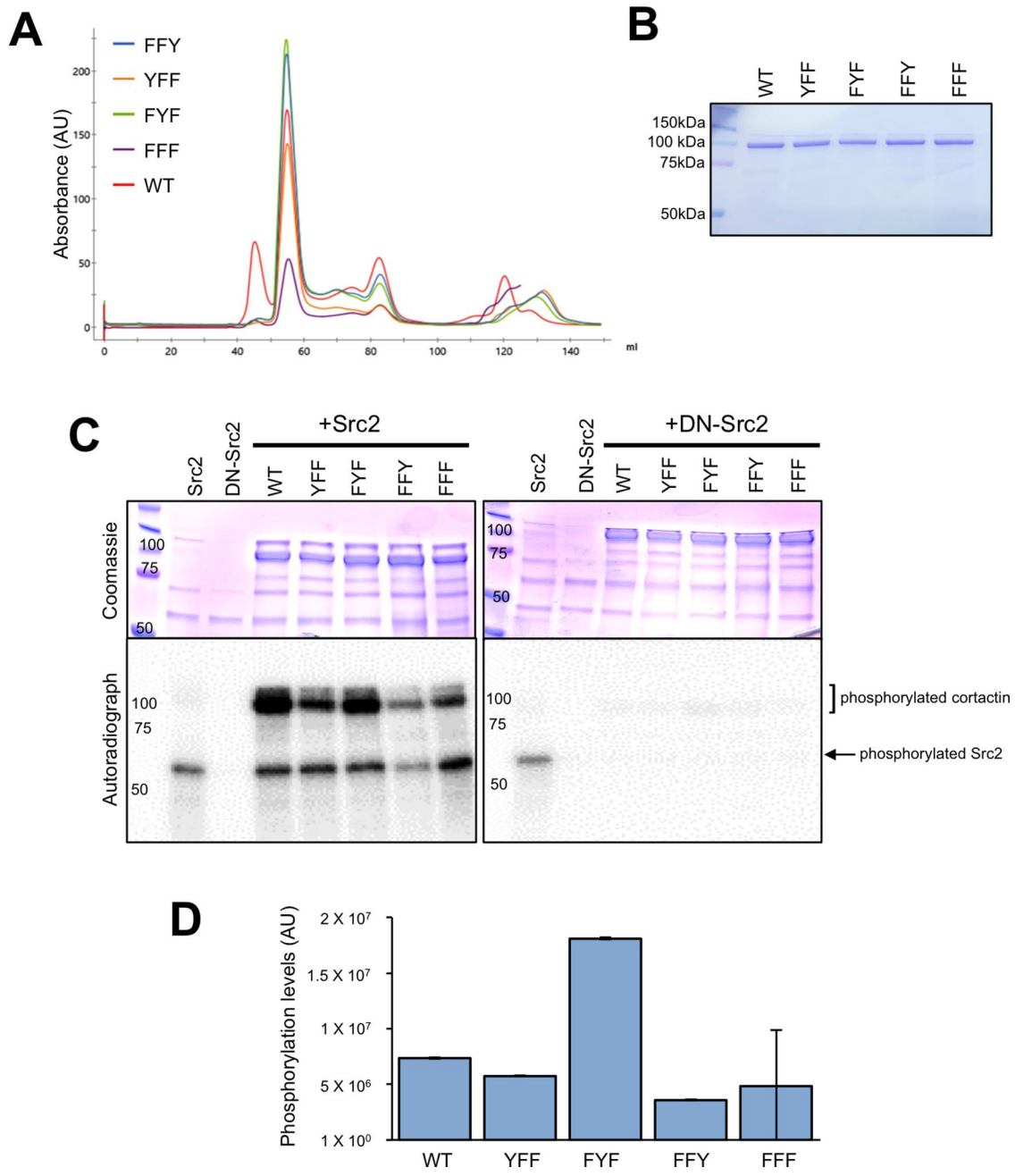

FIGURE 5: Src2 phosphorylates cortactin in vitro. (A) SEC profile of bacterially expressed and affinity-purified, recombinant WT and tyrosine phosphorylation mutants of cortactin (YFF, FYF, FFY, and FFF). The single peak at 55 ml elution volume corresponds to cortactin. Smaller peaks at 85 and 130 ml represent low molecular weight contaminants. WT cortactin also showed a second small peak at 45 ml, which may represent potentially oligomeric forms. (B) Coomassie-stained gel of WT and mutant cortactin proteins collected in the 55-ml elution volumes of the SEC peak in A. All samples show cortactin migrating as a doublet, with a predominant band corresponding to cortactin's molecular weight of 95 kDa and a fainter band at 110 kDa. (C) Autoradiograph and corresponding Coomassie-stained gel of a representative in vitro kinase reaction showing phosphorylation of WT or cortactin mutants by active Src2 or enzymatically dead dominant negative DNSrc2. Bands corresponding to phosphorylated Src2 (~65kDa) and phosphorylated cortactin (95–110 kDa doublet) are indicated. (D) Quantification of the average phosphorylation-specific signal associated with WT or mutant cortactin from four independent in vitro kinase reactions (mean ± SEM).

control verifying the lack of nonspecific cortactin phosphorylation (Figure 5C, right gel). Interestingly, mutation of putative tyrosine phosphorylation sites on *Aplysia* cortactin abrogated Src2-mediated tyrosine phosphorylation to varying levels. Phosphorylation of WT and mutant cortactin from four separate reactions was quantified. We found that while all three tyrosines (Y499, Y505, and Y509) can be phosphorylated by Src2, Y499 and Y505 are the preferred phosphorylation sites in vitro (Figure 5, C and D). Y509 can also be phosphorylated but seems to be less preferred. The triple mutant FFF still showed some phosphorylation, likely because Src2 phosphorylated secondary nonspecific sites on cortactin, as is commonly seen for kinases and other ATP-specific enzymes (Tagliabracci *et al.*, 2012;

Sanyal *et al.*, 2015). Interestingly, cortactin YFF showed reduced phosphorylation, while cortactin FYF exhibited enhanced phosphorylation, suggesting that unlike phenotypes seen in cells, Y499 does not appear to be the preferred site of phosphorylation in vitro. Instead, it appears that in the absence of Y499 and Y509, Y505 is preferentially phosphorylated. Together, these data provide the first evidence that *Aplysia* Src2 directly phosphorylates *Aplysia* cortactin and further highlight the possibility of cross-talk between three putative tyrosine phosphorylation sites in *Aplysia* cortactin.

Phosphorylated cortactin is part of a membrane-associated complex that promotes filopodia formation

Next, we tested whether the leading edge localization of phosphorylated cortactin is F-actin–dependent. To address this question, we treated the growth cones with either cytochalasin B or latrunculin A, both of which have been used to reversibly induce F-actin disassembly in *Aplysia* bag cell growth cones (Burnette *et al.*, 2007; Prager-Khoutorsky and Spira, 2009). Low dose of cytochalasin B (350–500 nM) results in selective removal of filopodia (Burnette *et al.*, 2007). Here, we applied either actin polymerization drug in a time-controlled manner to study the potential change in p-cort signal following F-actin disruption. Figure 6, A–D, shows a complete set of drug treatments, where growth cones were fixed and stained after treatment with either low ionic strength artificial sea water (LIS-ASW) plus 0.1% dimethyl sulfoxide (DMSO) (Figure 6, A–A‴; Supplemental Video 1) for 2 min, 500 nM cytochalasin B for 2 min (Figure 6, B–B‴; Supplemental Video 2), 500 nM cytochalasin B for 5 min (Figure 6, C–C‴; Supplemental Video 2), or 2 min washout with LIS-ASW after treatment with 500 nM cytochalasin B for 5 min (Figure 6, D–D‴; Supplemental Video 3). As expected, filopodia disappeared in a progressive manner with cytochalasin B treatment and regenerated within 2 min after drug removal (Figure 6, A–D), concurrent with the gradual loss and reappearance of F-actin and cortactin signals in the P-domain following drug washout (Figure 6, A′–D′). Interestingly, the p-cort signal persisted more at the leading edge throughout treatments (Figure 6, A″–D″), again displaying a different behavior than total cortactin (Figure 6, A‴–D‴). We quantified the changes of cortactin, F-actin, and p-cortactin throughout the drug treatment (Figure 6, I and J) and separated the P-domain into "Edge" and "Interior" to highlight the differentially regulated cortactin phosphorylation at different locations in the growth cone. We found that a fraction of cortactin is resistant to continued F-actin disassembly only at the leading edge (Figure 6I; only the nonsignificant difference is shown for clarity), and that cytochalasin B treatment increased cortactin phosphorylation ratio in both leading edge and P-domain interior (Figure 6J). This suggests an F-actin–independent localization of p-cortactin but not cortactin. Owing to the existence of a narrow cytochalasin B–resistant F-actin band at the leading edge, we cannot fully exclude the possibility that this phosphorylated cortactin is anchored through an interaction with F-actin. To determine whether this localization of phosphorylated cortactin is truly F-actin–dependent, we treated growth cones with 1 µM latrunculin A for 2 min (Figure 6, E–E‴) and 5 min (Figure 6, F–F‴) before probing the localization of F-actin, p-cort, and total cortactin. Similar to the cytochalasin B treatment, clearing of filopodia and F-actin with latrunculin A was still progressing at 2 min (Figure 6E, E′) and became complete by 5 min (Figure 6, F and F′). By the end of the 5-min latrunculin A treatment, both phosphorylated (Figure 6F″) and total cortactin (Figure 6F‴) was still visible at the leading edge, whereas no F-actin signal was detectable (Figure 6F′). These results strongly suggest that the localization of phosphorylated cortactin at the leading edge is independent of F-actin, possibly through its interaction with other membrane-associated proteins.

Because inhibition of Src activity reduced cortactin phosphorylation (Figure 3), we added PP2 to the actin drug washout solution to test the importance of Src-mediated cortactin phosphorylation for filopodia regeneration. Growth cones were fixed either after 1-min washout with LIS-ASW plus 0.1% DMSO following 500 nM cytochalasin B treatment (Figure 6, G–G‴) or after 1-min washout with LIS-ASW plus 25 µM PP2 following 500 nM cytochalasin B plus 25 µM PP2 treatment (Figure 6, H–H‴). In agreement with previous results, the p-cort band remained at the leading edge in the absence of PP2 (Figure 6G″); however, it was completely removed when Src was inhibited with PP2 (Figure 6H″). Meanwhile, the reappearing F-actin band behind the leading edge, which indicates the regenerating filopodial bundles and F-actin network, became narrower in PP2-treated growth cones (Figure 6, G′ and H′, quantification in K), suggesting that filopodia and lamellipodia formation is Src-dependent. Therefore, the leading edge localization of Src-phosphorylated cortactin appears to be critical for promoting filopodia formation in neuronal growth cones.

Arp2/3 complex acts downstream of cortactin to regulate filopodia density but not length

Owing to the importance of Arp2/3 complex in actin organization and dynamics, and the known role of cortactin in Arp2/3 complex activation (Weed *et al.*, 2000; Weed and Parsons, 2001; Uruno *et al.*, 2001; Weaver *et al.*, 2001; Schnoor *et al.*, 2018), we investigated whether Arp2/3 complex activation acts downstream of phosphorylated cortactin to regulate filopodia formation. To that end, we expressed cortactin NTA domain as dominant negative Arp2/3 inhibitor, or the cortactin FFF mutant as dominant negative construct for cortactin tyrosine phosphorylation in cultured *Aplysia* bag cell neurons by microinjection of mRNA (Figure 7, A–E and A′–E′, quantification in F and G). Similarly to the CA domain derived from N-WASP, the NTA domain derived from cortactin has been used as dominant negative Arp2/3 inhibitor (Komano *et al.*, 2004; Strasser *et al.*, 2004). As shown in Figure 7F, both NTA and cortactin FFF overexpression decreased filopodial density when expressed individually. However, no further decrease in filopodial density was detected when NTA was coexpressed together with cortactin FFF, suggesting that preventing cortactin-mediated activation of Arp2/3 complex in the background of cortactin that cannot be phosphorylated by Src tyrosine kinase cannot further decrease filopodial density. These results suggest Src-mediated phosphorylation of cortactin and activated Arp2/3 complex likely function in the same pathway to regulate filopodial density through the formation and/or stabilization of filopodia. On the other hand, NTA expression did not decrease filopodial length, whereas cortactin FFF expression did in agreement with our earlier findings (Figure 7G). These findings suggest that Src-mediated phosphorylation of cortactin controls filopodial length through a pathway that does not involve the Arp2/3 complex, which is consistent with an expected role of the Arp2/3 complex in actin nucleation in lamellipodial network but not at the filopodial tips.

DISCUSSION

Src is a nonreceptor tyrosine kinase involved in several cellular activities such as cell division, migration, proliferation, adhesion, and cell survival (Parsons and Parsons, 2004; Roskoski, 2004; Aleshin and Finn, 2010). In neuronal growth cones, Src transduces signals from receptors for cues such as netrin, brain-derived neurotrophic factor, ephrinA, and apCAM to actin during axonal growth and guidance (Suter and Forscher, 2001; Knoll and Drescher, 2004; Li *et al.*, 2004;

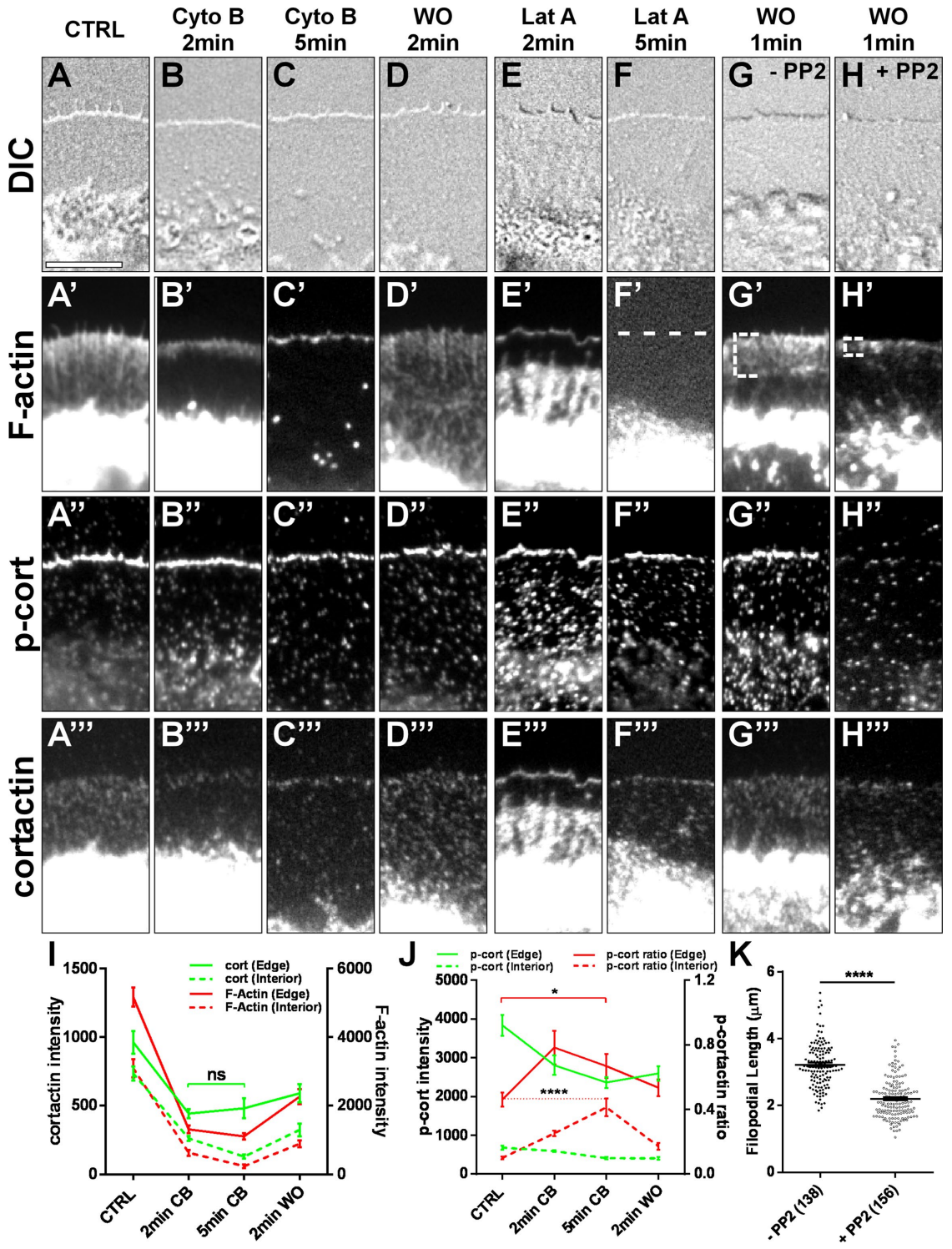

FIGURE 6: Phosphorylated cortactin is part of a membrane-associated complex that promotes filopodia formation. Localization of F-actin, phosphorylated cortactin, and total cortactin in the growth cone P-domain after treatment with LIS-ASW and 0.1% DMSO (CTRL, A–A‴), 500 nM cytochalasin B (Cyto B) for 2 min (B–B‴), 500 nM Cyto B for 5 min (C–C‴), 2 min washout with LIS-ASW after 500 nM Cyto B for 5 min (D–D‴), 1 μM latrunculin A (Lat A) for 2 min (E–E‴), 1 μM Lat A for 5 min (F–F‴), 1 min washout with LIS-ASW after 500 nM Cyto B for 5 min (G–G‴), 1 min washout with LIS-ASW plus 25 μM PP2 after 500 nM Cyto B plus 25 μM PP2 for 5 min (H–H‴). (A–D) Filopodia disappear after 5 min Cyto B treatment and regenerate in 2 min after washout (WO). (E, F) Lat A treatment for 5 min completely eliminated F-actin from the P-domain, but did not remove p-cortactin signal at the leading edge. (G, H) Regeneration of filopodia after Cyto B treatment was reduced by PP2 treatment, concurrent with a loss of p-cortactin signal from leading edge, suggesting that phosphorylated cortactin at the leading edge promotes filopodia formation. Dash line in F′ denotes P-domain edge; brackets in G′ and H′ indicate regenerated filopodia. (I, J) Analysis of cortactin intensity, p-cortactin intensity, F-actin intensity, and p-cortactin ratio for A–D. Edge is defined as a 1-μm band at the leading edge

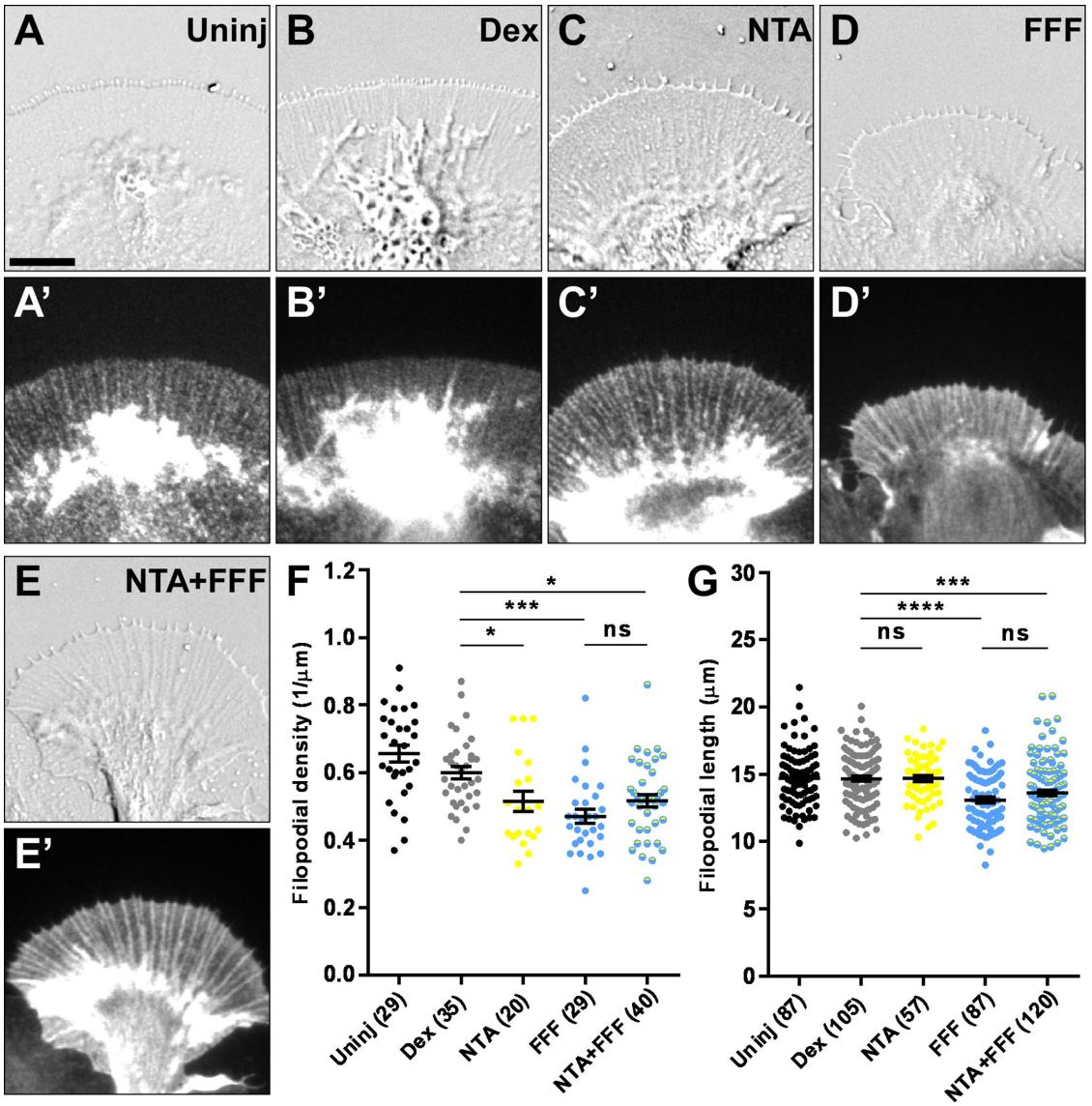

FIGURE 7: Phosphorylated cortactin to Arp2/3 signaling controls filopodial density but not length. (A–E) DIC images of growth cones following expression of different cortactin constructs. (A′–E′) Immunostaining of total cortactin with 4F11 antibody. (F) Whereas individual NTA and FFF overexpression significantly reduced filopodia density, the coexpression of NTA and FFF did not reduce filopodial density further, suggesting that phosphorylated cortactin and Arp2/3 are in the same signaling pathway with respect to filopodia formation/stability. Numbers in parentheses are numbers of growth cones analyzed. (G) Only FFF but not NTA overexpression decreased filopodia length. This suggests that cortactin phosphorylation but not Arp2/3 plays a role in controlling the length of filopodia. Numbers in parenthesis are numbers of filopodia analyzed. Data in F and G are presented as mean ± SEM and are representative of two independent experiments. *$P < 0.05$; ***$P < 0.001$; ****$P < 0.0001$. ANOVA with Dunnett's multiple comparison. Scale bar: 10 µm.

Liu *et al.*, 2004; Robles *et al.*, 2005). Following activation near the cell membrane, Src functions by phosphorylating key substrate proteins like cortactin (Liu *et al.*, 1999). Recent evidence suggests that cortactin is involved in lamellipodia protrusion, filopodia formation, and stabilization in neuronal growth cones (Kurklinsky *et al.*, 2011; Yamada *et al.*, 2013; He *et al.*, 2015; Kubo *et al.*, 2015). For example, it was proposed that cortactin and dynamin-1 form ringlike structures that stabilize actin bundles in growth cone filopodia (Yamada *et al.*, 2013). Src-mediated phosphorylation is critical for cortactin's role in actin regulation in vitro or in nonneural cells (Nieto-Pelegrin and Martinez-Quiles, 2009; Cao *et al.*, 2010; Navratil *et al.*, 2014; Radhakrishnan *et al.*, 2014). However, the role of cortactin

of growth cone; interior is P-domain minus the leading edge. Cortactin phosphorylation ratio was increased with F-actin removal, indicating an F-actin–independent retention of p-cortactin but not total cortactin. (K) Quantification of regenerated filopodia length for G and H. Inhibition of cortactin phosphorylation significantly reduced regenerated filopodial length. Data are presented as mean ± SEM and are representative of six independent experiments. Numbers in parenthesis are numbers of growth cones analyzed. *$P < 0.05$; ****$P < 0.0001$. ANOVA with Dunnett's multiple comparison for J; unpaired *t* test for K. Scale bar: 5 µm.

phosphorylation by Src in neuronal growth cones has only recently been elucidated by work from our group (He *et al.*, 2015).

Src2 is one of two Src tyrosine kinases identified in *Aplysia* (Wu *et al.*, 2008). Using high-resolution imaging of live neurons, we showed that up-regulation of either Src2 or cortactin led to more and longer filopodia in the P-domain of *Aplysia* growth cones, as well as to an increase in the density of the actin-based network in lamellipodia. Conversely, down-regulation of Src2, or the overexpression of a phosphorylation-defective triple tyrosine mutant (FFF) of cortactin, resulted in fewer and shorter filopodia, increased lateral movement of filopodia, as well as decreased network density of lamellipodia (He *et al.*, 2015). In our current study, we provide the first biochemical evidence that *Aplysia* Src2 directly phosphorylates *Aplysia* cortactin in vitro (Figure 5). Further, we identified Y499 in the proline-rich domain of *Aplysia* cortactin as the functional tyrosine residue that mediates the effect of phosphorylated cortactin on filopodia formation. Cortactin 499F phenocopied cortactin FFF in reducing filopodial density and length (Figure 1, J and K), and 499E increased filopodial length to comparable levels as EEE (Figure 2J). Moreover, overexpression of the cortactin FEE mutant reduced filopodial density and length, whereas overexpression of the cortactin EFF mutant increased filopodial length (Figure 2, K and L). These results suggest that cortactin Y499 is the only relevant tyrosine residue whose phosphorylation state dictates the function of cortactin on filopodia formation. Furthermore, our data with p-cort antibody demonstrated that Src2 phosphorylated cortactin at Y499 in vivo (Figures 3 and 4). The drop in cortactin tyrosine phosphorylation ratio when overexpressing WT cortactin (Figure 4T) suggests that cortactin phosphorylation could be tightly regulated possibly by a limited pool of active Src2 in growth cones. In agreement, our in vitro phosphorylation data (Figure 5, C and D) suggest cross-talk between phosphorylation at Y505 and at sites Y499 and Y509, where Y505 displayed high phosphorylation levels when Y499 and Y509 were mutated. Alternatively, the overexpressed cortactin in cells might also oligomerize, thereby masking the phosphorylation site, a hypothesis corroborated by the presence of a small oligomeric peak for WT cortactin during SEC purification (Figure 5A). In summary, we have characterized a key phosphorylation site on cortactin, which serves as an important switch in communicating Src kinase activity to actin reorganization in neuronal growth cone.

Murine cortactin can be phosphorylated at Y421, Y466, and Y482 by Src family kinases, where the phosphorylation of Y466 and Y482 happens in a progressive manner after the initial phosphorylation of Y421 (Huang *et al.*, 1998; Head *et al.*, 2003; Nieto-Pelegrin and Martinez-Quiles, 2009). Functional analysis found that phosphorylation of Y421 and Y466, but not Y482, is important in generating free actin barbed ends in invadopodia formation (Oser *et al.*, 2010; Rosenberg *et al.*, 2017). In cancer cells, a pool of constitutively phosphorylated cortactin Y421 becomes further phosphorylated at Y470 (the human equivalent of mouse Y466), which is sufficient for the redistribution of cortactin to cell adhesion sites (Hoye *et al.*, 2016). For *Aplysia* cortactin, a sole phosphorylation/dephosphorylation event at Y499 seems to be responsible for the altered behavior of cortactin on actin remodeling, at least in the context of filopodia formation (Figure 2, K and L). Based on sequence alignments of *Aplysia* with mouse and human cortactin, it is difficult to determine which of the Y421, Y466, and Y482 tyrosine residues is the functional equivalent of Y499 in *Aplysia* cortactin. The multiple tyrosine phosphorylation events and subsequent divergence in activities of differently phosphorylated cortactin could be a product of evolution to fine tune cortactin functions. Our in vitro data revealed some interesting differences to our cell biological data. In contrast to living neurons, where phosphorylation of Y499 appears to have to the most significant phenotypic effects, our in vitro kinase data suggest that Y505 is preferentially modified versus Y499 (Figure 5). Such differences in phosphorylation pattern between in vitro and in vivo assays are not unexpected since 1) other involved proteins could be missing in the in vitro kinase assay and 2) kinases are known to phosphorylate more substrates in vitro than in vivo (Tagliabracci *et al.*, 2012; Sanyal *et al.*, 2015).

The localization of phosphorylated cortactin along the leading edge and filopodia tips of growth cones (Figure 3) is in agreement with the localization of active Src (Robles *et al.*, 2005; He *et al.*, 2015), as well as with the role of cortactin in promoting filopodia formation from submembrane regions. Few studies have localized tyrosine-phosphorylated cortactin in cells so far. pY421 cortactin is enriched at the leading edge of smooth muscle cells and human breast cancer cells following growth factor stimulation (Mezi *et al.*, 2012; Cleary *et al.*, 2014). Other key actin regulators, including N-WASP, formin, and Ena/VASP, are also localized at the leading edge to control actin organization and dynamics, where phosphorylated cortactin may interact to control filopodia density and length (Small *et al.*, 2002; Faix and Rottner, 2006; Mellor, 2010). Direct binding to actin-binding proteins (Nieto-Pelegrin and Martinez-Quiles, 2009; Weidmann *et al.*, 2016) or the structural integrity of F-actin itself (Abedi and Zachary, 1998; Di Ciano *et al.*, 2002; Fan *et al.*, 2004) may also regulate cortactin phosphorylation. Indeed, cortactin phosphorylation at the growth cone leading edge seems to be under tight spatial control, as the phosphorylation ratio quickly drops to background level just a few micrometers away from the growth cone leading edge (Figures 3D and 4, D and H). Phosphorylated cortactin is enriched along filopodia that protrude outside of the leading edge, but not along the filopodia shaft embedded in the lamellipodia (Figure 3M). Along the leading edge and inside the filopodia, phosphorylated cortactin seems to be clustered, hinting at the possibility of higher-order structures (hot spots in Figure 3, D and M; Figure 4, D and H) (Yamada *et al.*, 2013; He *et al.*, 2015). Hot spots of p-cort signal away from the leading edge may reflect active endocytic sites, which have been shown to involve cortactin tyrosine phosphorylation (Zhu *et al.*, 2007; Cao *et al.*, 2010). Cortactin phosphorylation signal is quickly lost with short time inhibition of Src2 activity (15 min in Figure 3, H and K; 6 min in Figure 6H″), along with the disappearance of p-cort band from growth cone P-domain edge. This implies a fast dephosphorylation of cortactin, possibly by PTP1B phosphatase (Weidmann *et al.*, 2016) that works in concert with Src2 to control cortactin phosphorylation levels temporally. Once phosphorylated, however, cortactin becomes stably anchored at the leading edge to promote filopodia formation (Figure 6).

From in vitro studies, tyrosine phosphorylation of cortactin has been shown to promote actin assembly and branching, while reducing its F-actin cross-linking ability (Huang *et al.*, 1997; Tehrani *et al.*, 2007). This seems to be consistent with our data, where phosphorylated cortactin localizes only at the "birth place" of filopodia, where enhanced actin assembly and branching increases the length and number of filopodia, and unphosphorylated cortactin binds along F-actin bundles in filopodia shafts to potentially stabilize filopodia. Unphosphorylated cortactin is thought to exist in a "closed" conformation with an intramolecular interaction between its proline-rich domain and SH3 domain (Cowieson *et al.*, 2008; Evans *et al.*, 2012; Schnoor *et al.*, 2018). Whether Src-phosphorylated cortactin exists in closed or open conformation in vivo is unknown. Our data suggest that the majority of unphosphorylated cortactin may be in a closed conformation in neuronal growth cones, with Y499, Y505,

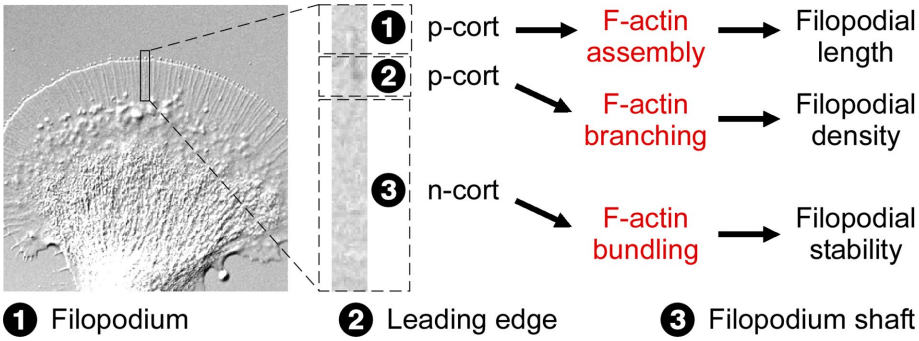

FIGURE 8: Summary of proposed cortactin functions in filopodia formation. One growth cone filopodium is highlighted and separated into three regions: filopodium outside veil, leading edge, and filopodium shaft, where different aspects of filopodia behavior are regulated. Phosphorylated cortactin mainly localizes at filopodium tip and the leading edge to promote F-actin assembly and branching, leading to the formation of longer and denser filopodia. In contrast, unphosphorylated cortactin binds to bundled F-actin in the interior of growth cone P-domain, which helps to stabilize filopodia. The local binding partners of different species of cortactin need to be further identified.

and Y509 protected by the SH3 domain interacting with the proline-rich region. Therefore, the n-cort antibody is expected to detect cortactin only in the open but not closed conformation. This is indeed what we observed in our experiments. The n-cort antibody detected denatured cortactin protein in the Western blot (Supplemental Figure S1, C, and D), but failed to detect strong signals in the growth cone P-domain or along the filopodia shaft, where the majority of cortactin is hypothesized to be in an unphosphorylated state (compare Figure 3, B and C, with Supplemental Figure S2O). Src-mediated cortactin phosphorylation may be a subsequent step of cortactin unfolding to help maintaining an open conformation. Although the direct interaction between Src phosphorylated cortactin and N-WASP appears to be decreased based on previous studies, tyrosine-phosphorylated cortactin could bind WIP with its SH3 domain to indirectly synergize with N-WASP to promote actin branching, as well as recruit SH2-containing adaptor proteins such as Nck to activate N-WASP (Martinez-Quiles *et al.*, 2001; Kinley *et al.*, 2003; Lua and Low, 2005; Tehrani *et al.*, 2007). The availability of cortactin SH3 domain could also recruit other proline-rich domain containing proteins such as dynamin to form special structures along filopodia (Yamada *et al.*, 2013). Dynamin may help localize phosphorylated cortactin at the P-domain edge, even in the absence of F-actin (Figure 6, F–F‴).

Although traditionally viewed as a nucleation promoting factor, at least some of cortactin's function can be exerted independent of its NTA domain, highlighting the scaffolding role of cortactin in actin remodeling (Olazabal and Machesky, 2001; Ayala *et al.*, 2008; Lai *et al.*, 2009; Magalhaes *et al.*, 2011). We found that interfering with cortactin phosphorylation and Arp2/3 complex at the same time did not further decrease filopodia density compared with interfering with one mechanism alone, suggesting that phosphorylated cortactin may act through the Arp2/3 complex to regulate filopodia formation and density (Figure 7A). Phosphorylated cortactin could either synergize with N-WASP through the aforementioned mechanisms to promote actin branching or accelerate the release of cofilin to create more barbed ends to serve as precursors of filopodia (Oser *et al.*, 2009, 2010; Magalhaes *et al.*, 2011; Helgeson and Nolen, 2013). In contrast, inhibition of Arp2/3 complex activation alone had no direct effect on filopodia length, pointing to the possibility that cortactin utilizes other binding partners to control filopodia length (Figure 7G). Considering that filopodia elongation is governed mainly by actin regulators at the plus end of actin bundles, phosphorylated cortactin may recruit formin to promote actin polymerization, as shown recently in invadopodia formation (Ren *et al.*, 2018).

In summary, we have identified a critical Src-mediated tyrosine phosphorylation of *Aplysia* cortactin Y499 regulating filopodia formation (Figure 8). Tyrosine-phosphorylated cortactin localizes at the growth cone leading edge and filopodia tips, where it likely partners with Arp2/3 complex and proteins in the filopodial tip complex to regulate filopodial density and length, respectively. In contrast, unphosphorylated cortactin mainly binds along F-actin bundles in the filopodium shaft to promote filopodial stability. The exact molecular mechanism of cortactin-dependent filopodia formation and maintenance, and the binding partners of cortactin within subdomains of filopodia, requires further exploration.

MATERIALS AND METHODS

Cell culture

Aplysia bag cell neurons were collected from Dispase-digested abdominal ganglion of 150–200 g *Aplysia californica* (Marinus Scientific, Long Beach, CA) and plated on a 20 μg/ml poly-L-lysine (70–150 kDa; Sigma-Aldrich, St. Louis, MO)-coated glass coverslip as described previously (Lee *et al.*, 2008; He *et al.*, 2015). Culture media were made by adding artificial seawater (ASW) into commercially available L15 media (Invitrogen, Life Technologies, Grand Island, NY). Final solution (L15-ASW) contains 400 mM NaCl, 9 mM $CaCl_2$, 27 mM $MgSO_4$, 28 mM $MgCl_2$, 4 mM L-glutamine, 50 μg/ml gentamicin, 5 mM HEPES, pH 7.9, 950–1000 mOsm. For better solubility of Src-inhibitor PP2 (Sigma) dissolved in DMSO, we used LIS-ASW, which contains 100 mM NaCl, 10 mM KCl, 5 mM $MgCl_2$, 5 mM $CaCl_2$, 15 mM HEPES, and 60 g/l glycine, pH 7.9, 950-1000 mOsm.

mRNA-mediated protein overexpression

Constructs for overexpression of WT *Aplysia* cortactin, triple tyrosine phosphorylation cortactin mutant FFF (named CortF in our recent publication [He *et al.*, 2015]), and WT Src2 in pRAT expression vector were described previously (Wu *et al.*, 2008; He *et al.*, 2015). Using the QuikChange II site-directed mutagenesis kit (Agilent Technologies, Santa Clara, CA), we created the following additional cortactin mutants: single tyrosine phosphorylation mutants 499F, 505F, and 509F; single phospho-mimetic mutant 499E; triple phospho-mimetic mutant EEE (499E/505E/509E); as well as the following two combinations of phosphorylation and phospho-mimetic mutants: FEE (499F/505E/509E) and EFF (499E/505F/509F). All constructs were confirmed by sequencing. mRNAs for overexpression of *Aplysia* proteins were made using the mMESSAGE mMACHINE T7 and the mMESSAGE mMACHINE T7 Ultra in vitro transcription kit (Ambion, Life Technologies, Grand Island, NY). This Ultra kit generates mRNAs that result in twofold higher protein levels in *Aplysia* neurons when compared with mRNAs created by the standard version of the kit. A typical final concentration of 0.5 mg/ml mRNA was mixed with dextran (3kD Texas red dextran, fixable; Thermo Fisher Scientific) and delivered into soma through microinjection typically 4 h after cell plating. NP2 micromanipulator and FemtoJet microinjection system

(Eppendorf, Hauppauge, NY) were used together with Nikon TE2000-U Eclipse inverted microscope to inject *Aplysia* neurons. Either dextran or Tris/EDTA buffer injections served as controls in addition to uninjected neurons. Injected neurons were given an additional 24 h for adequate protein expression and growth cone formation. Immunostaining of growth cones with the monoclonal cortactin antibody 4F11 (Millipore, Billerica, MA) was used to ensure that only growth cones with 50%–200% overexpression of cortactin higher than control growth cones were used for subsequent analysis of effects of cortactin overexpression. Staining of total cortactin in growth cones is shown in Figures 1–4, 6, and 7.

Immunocytochemistry

A pY499 phospho-cortactin-specific antibody was raised in rabbit against the following cortactin peptide sequence (amino acids 493–504): PERVEDpYGEETE (Pacific Immunology, Ramona, CA). The antiserum was first purified against the nonphosphorylated peptide to yield the n-cort antibody specific to nonphosphorylated cortactin and then against the phosphorylated peptide to yield the p-cort antibody specific to phosphorylated cortactin. Affinity-purified antibody stock solutions were prepared in 1.5 mg/ml (for n-cort antibody) and 0.8 mg/ml (for p-cort antibody) phosphate-buffered saline (PBS)/0.01% NaN_3. Growth cones were fixed with 3.7% formaldehyde in ASW plus 400 mM sucrose for 15 min at room temperature, before permeabilization with fixation solution plus 0.05% saponin for 10 min. After several washing with PBS/0.005% saponin, samples were blocked with 5% bovine serum albumin (BSA) in PBS/saponin for 1 h at room temperature. Primary antibodies were diluted in blocking buffer and incubated with samples for 2 h at room temperature. The 4F11 cortactin antibody was typically used at 2 µg/ml, p-cort at 4 µg/ml, and n-cort at 8 µg/ml. Goat anti-rabbit Alexa-568– and goat anti-mouse Alexa-647–conjugated secondary antibodies (A-11011 and A-21235; Thermo Scientific, Waltham, MA) were diluted in PBS/saponin, typically at 2 µg/ml, and incubated with samples for 1 h at room temperature. For peptide blocking, 5 µg peptide was used for every microgram of antibody and added into primary antibody solution during sample incubation. Alexa-488 Phalloidin (A12379; Thermo Scientific, Waltham, MA) diluted with PBS/0.005% saponin to a final concentration of 66 nM and incubated for 30 min at room temperature to label F-actin. Phalloidin labeling was done before antibody labeling.

Microscopy

Coverslips with cells were assembled into imaging chambers as described previously (Lee *et al.*, 2008). Samples were imaged on Nikon TE2000 E2 inverted microscope (Nikon, Melville, NY) with 60× oil-immersion objective plus additional 1.5× magnification. X-cite 120 metal halide lamp (EXFO, Quebec City, QC, Canada) and corresponding filter sets (Chroma Technology, Bellows Falls, VT) were used for fluorescence imaging. Digital acquisition was supported by an Andor iXon 888 Ultra electron-multiplying charge-coupled device camera under the control of MetaMorph 7.8 software (Molecular Devices, Sunnyvale, CA). DIC time-lapse imaging was carried out at 5-s intervals.

STORM imaging

dSTORM was performed on a custom setup built around an Olympus IX-73 microscope stand (IX-73; Olympus America, Waltham, MA) using a 100×/1.35 NA silicone oil-immersion objective lens (FV-U2B714; Olympus America) and a PIFOC objective positioner (ND72Z2LAQ; Physik Instrumente, Karlsruhe, Germany). Sample excitation and activation were achieved with a 642-nm laser (2RU-VFL-P-2000-642-B1R; MPB Communications, Pointe Claire, QC, Canada) and a 405-nm laser (DL-405-100; Crystalaser, Reno, NV), respectively. Both lasers were focused to the back aperture of the objective lens and offset from the optical axis so that the sample was illuminated in HILO mode (Tokunaga *et al.*, 2008). The filter turret contained a quad band dichroic mirror (Di03-R405/488/561/635-t1; Semrock, Rochester, NY) for illumination with both lasers. Relay lenses arranged in a 4*f* alignment resulted in a final magnification of 52.7 at the sCMOS camera (Orca-Flash4.0v3, Hamamatsu, Tokyo, Japan) with an effective pixel size of 120 nm. The fluorescence signal passed through a bandpass filter (FF01-731/137-25; Semrock) placed just before the camera. Localization of single molecules was performed as described previously (Huang *et al.*, 2013).

Image analysis

Morphological analysis of filopodia density and length was conducted in the P-domain of growth cones. Filopodial density is defined as the average number of filopodia per unit length of leading edge. Filopodial length is calculated by measuring the distance between the filopodia tip protruding outside the leading edge and the filopodia base inside the lamellipodia close to the transition zone and visible in both DIC and fluorescent images of F-actin or cortactin labeling. Ratiometric images were created by using the Ratio Plus plug-in in ImageJ (National Institutes of Health [NIH], Pasadena, MD). Fluorescence intensity in growth cone P-domain was quantified after background subtraction using MetaMorph 7.8 (Molecular Devices, Sunnyvale, CA).

Western blotting

Aplysia CNS lysate was prepared by homogenizing whole CNS from adult *Aplysia* with an Omnimixer (Omni International, Kennesaw, GA) in lysis buffer (50 mM Tris-HCl, 150 mM NaCl, 2 mM EGTA [ethylene glycol-bis(β-aminoethyl ether)-*N*,*N*,*N*′,*N*′-tetraacetic acid], 2 mM EDTA, 1% Triton X-100, 0.5 mM Pefabloc SC Plus [Roche, Indianapolis, IN], 1% protease inhibitor cocktail [Sigma], 1 mM Na_3VO_4, 10 mM NaF, and 20 mM beta glycerophosphate, pH 7.5) and centrifuged at 10,000 × *g* for 30 min at 4°C. Only the supernatant was collected for gel analysis. In the PP2 treatment group, a final concentration of 25 µM PP2 (Sigma) was added during homogenization process. Lysates were separated by SDS–PAGE on a 7.5% gel and then transferred onto a polyvinylidene difluoride membrane. Blocking was performed with 10% fetal bovine serum (FBS) in PBS containing 4 mM Na_3VO_4 and 50 mM β-glycerophosphate for 1 h at room temperature. For primary antibody incubation overnight at 4°C, 3.2 µg/ml p-cort or 6 µg/ml N-cort antibody was added to PBS with 0.05% Triton X-100 (PBST) containing 5% FBS, 4 mM Na_3VO_4, 50 mM β-glycerophosphate, along with 2 µg/ml diluted 4F11. After washing with 0.1% PBST, the membrane was incubated with 0.2 µg/ml goat anti-rabbit 680 antibody (Thermo Scientific) for p-cort or n-cort together with 0.2 µg/ml goat anti-mouse 800 antibody (Thermo Scientific) for 4F11 in PBST containing 5% FBS, 0.01% SDS, 4 mM Na_3VO_4, and 50 mM β-glycerophosphate for 1 h at room temperature. Following extensive washing of the membrane with 0.1% PBST, signals were detected on an Odyssey imaging system (LI-COR Biosciences, Lincoln, NE). For peptide blocking experiments, 5 µg peptide was used for every microgram of antibody during primary antibody incubation.

Constructs for bacterial expression of *Aplysia* cortactin and Src2 proteins

To express full-length *Aplysia* cortactin proteins, pQE-30UA plasmids containing either WT cortactin or putative Src2 phosphorylation site mutants (YFF, FYF, FFY, or FFF) template DNA were

amplified with PCR using the primers 5′-GCTGGAGGATCCATGCCACGTGATATCCTCAATCGC-3′ and 5′-CGACGTCTCGAGTTACTGCTGCAGCTCCACGTAG-3′. PCR products were digested with *Xho*1 and *Bam*HI and cloned as N-terminal His_6-SUMO fusion into pSMT3 expression vector (Sanyal *et al.*, 2015). Each construct was verified by restriction digestion and DNA sequencing. Both Src2 kinase and the DNSrc2 (He *et al.*, 2015) were cloned into pET-Duet with an N-terminal His_6-tag. GST-tagged, truncated *Yersinia* YopH phosphatase (yop51Δ184*; missing 184 residues at the N-terminal and an Arg in place of Ser at position 235) was cloned into the plasmid pT7-7 (Zhang *et al.*, 1992).

Protein expression and purification

pET-Duet, His_6-SUMO fusion, and GST-fusion (YopH) constructs were transformed into *Escherichia coli* BL21-DE3-competent cells. Overnight *E. coli* cultures (10 ml) were grown from a single colony and used to inoculate 1 l of lysogeny broth media containing 50 µg/ml kanamycin (for pSMT3) or 100 µg/ml ampicillin (for pT7-7 or pET-Duet). Cultures were grown at 37° C to OD_{600} of 0.6–0.9, induced with 0.4 mM IPTG (isopropyl *p*-thiogalactoside), and grown for an additional 4 h at 37° C. Any phosphorylation of induced proteins by bacterial ATP was eliminated by copurifying YopH phosphatase with cultures of overexpressed cortactin or kinase (Src2 or DNSrc2) in a 1:2 ratio and 1:1 ratio, respectively. The cells were harvested by centrifugation at 7500 × *g* for 10 min. The resulting pellets were resuspended in lysis buffer (50 mM Tris, pH 8.0, 300 mM NaCl, 20 mM imidazole, 5 mM β-mercaptoethanol [BME], 0.5% Triton X-100, 10% glycerol) supplemented with 5 mM phenylmethylsulfonyl fluoride protease inhibitor and sonicated on ice for 4 min at 30-s intervals. The soluble fraction was isolated by centrifuging the lysates at 15,000 rpm for 35–40 min at 4° C and loaded onto 4–6 ml of cobalt resin (Thermo Fisher). Binding of the His_6-tagged proteins to cobalt resin was accomplished by gentle shaking at 4° C for 1 h. Resin was washed with wash buffer twice (50 mM Tris, pH 8.0, 300 mM NaCl, 20 mM imidazole, 5 mM BME), and the protein of interest was eluted from the resin using elution buffer (100 mM Tris, pH 8.0, 150 mM NaCl, 300 mM imidazole, 10% glycerol). After measuring protein concentrations using A_{280} extinction coefficient, Bradford assay, and visualization by Coomassie against bovine serum albumin (BSA) standards, His-tagged purified Src2 kinases were confirmed via Western blotting using monoclonal anti-His antibody (Sigma Aldrich) and then concentrated using a 65 kDa cutoff Centricon column. Eluted cortactin fractions were further purified by SEC in buffer containing 10 mM Tris, pH 8.0, 100 mM NaCl. His-affinity-purified WT cortactin or its mutants were loaded onto a Hiload 16/600 Superdex 200 PG column (GE Healthcare, Chicago, IL) using an ÄKTA pure system at a flow rate of 1 ml/min. Total protein concentration was determined spectrophotometrically at 280 nm, as well as assaying the fractions using the Bradford Assay (BioRad Protein Assay Reagent and measuring the absorbance at 595 nm). Purity was confirmed by SDS–PAGE and comparison to known BSA standards. Proteins were stored at –80° C with 10% glycerol.

In vitro kinase assay

Phosphorylation reaction was performed with either SEC-purified His_6-SUMO-tagged WT or mutant cortactin alone or with Src2 or DNSrc2. In addition, WT Src2 or DNSrc2 was incubated alone to assess autophosphorylation reaction as a control. Proteins were incubated in the reaction buffer containing 50 mM Tris, pH 7.5, 5 mM $MgCl_2$, 5 mM $MnCl_2$, 1 mM dithiothreitol, 0.25 mM sodium orthovanadate (20-µl aliquots). The kinase reaction was initiated with 2.5 µCi γ-^{32}P-ATP and incubated for 20 min at 30°C. The reaction was quenched by the addition of SDS–PAGE loading buffer. Samples were separated by SDS–PAGE on 10% polyacrylamide gels and analyzed by autoradiography using film and the Typhoon phosphor-imager (GE Healthcare). Bands were quantified using Typhoon phosphor-imager and the associated ImageQuant program.

ACKNOWLEDGMENTS

We thank former lab members Boris Decourt and Melissa Casella for their help with the wild-type cortactin expression construct and initial protein purification. We thank Carol Post, Purdue University, for helpful discussions, and Jack Dixon, University of California, San Diego, for providing the YopH plasmid, yop51Δ184*. D.M.S. was supported by a grant from the National Science Foundation (1146944-IOS) and grants from the Purdue Research Foundation. F.H. was supported by grants from the NIH (R35-GM119785) and DARPA (D16AP00093). S.M. was supported by a grant from NIH (R01-GM10092). S.B. was supported by a Bird Stair Graduate Student Fellowship from the Department of Biochemistry, Purdue University.

REFERENCES

Abedi H, Zachary I (1998). Cytochalasin D stimulation of tyrosine phosphorylation and phosphotyrosine-associated kinase activity in vascular smooth muscle cells. Biochem Biophys Res Com 245, 646–650.

Aleshin A, Finn RS (2010). SRC: a century of science brought to the clinic. Neoplasia 12, 599–607.

Ammer AG, Weed SA (2008). Cortactin branches out: roles in regulating protrusive actin dynamics. Cell Motil Cytoskel 65, 687–707.

Athamneh AI, Suter DM (2015). Quantifying mechanical force in axonal growth and guidance. Front Cell Neurosci 9, 359.

Ayala I, Baldassarre M, Giacchetti G, Caldieri G, Tete S, Luini A, Buccione R (2008). Multiple regulatory inputs converge on cortactin to control invadopodia biogenesis and extracellular matrix degradation. J Cell Sci 121, 369–378.

Block J, Stradal TE, Hanisch J, Geffers R, Kostler SA, Urban E, Small JV, Rottner K, Faix J (2008). Filopodia formation induced by active mDia2/Drf3. J Microsc 231, 506–517.

Bryce NS, Clark ES, Leysath JL, Currie JD, Webb DJ, Weaver AM (2005). Cortactin promotes cell motility by enhancing lamellipodial persistence. Curr Biol 15, 1276–1285.

Burnette DT, Schaefer AW, Ji L, Danuser G, Forscher P (2007). Filopodial actin bundles are not necessary for microtubule advance into the peripheral domain of Aplysia neuronal growth cones. Nat Cell Biol 9, 1360–1369.

Cao H, Chen J, Krueger EW, McNiven MA (2010). SRC-mediated phosphorylation of dynamin and cortactin regulates the "constitutive" endocytosis of transferrin. Mol Cell Biol 30, 781–792.

Chan CE, Odde DJ (2008). Traction dynamics of filopodia on compliant substrates. Science 322, 1687–1691.

Cleary RA, Wang R, Waqar O, Singer HA, Tang DD (2014). Role of c-Abl tyrosine kinase in smooth muscle cell migration. Am J Phys Cell Phys 306, C753–C761.

Cosen-Binker LI, Kapus A (2006). Cortactin: the gray eminence of the cytoskeleton. Physiology 21, 352–361.

Cowieson NP, King G, Cookson D, Ross I, Huber T, Hume DA, Kobe B, Martin JL (2008). Cortactin adopts a globular conformation and bundles actin into sheets. J Biol Chem 283, 16187–16193.

Davenport RW, Dou P, Rehder V, Kater SB (1993). A sensory role for neuronal growth cone filopodia. Nature 361, 721–724.

Decourt B, Munnamalai V, Lee AC, Sanchez L, Suter DM (2009). Cortactin colocalizes with filopodial actin and accumulates at IgCAM adhesion sites in Aplysia growth cones. J Neurosci Res 87, 1057–1068.

Dent EW, Gupton SL, Gertler FB (2011). The growth cone cytoskeleton in axon outgrowth and guidance. Cold Spring Harb Perspect Biol 3, a001800.

Dent EW, Kwiatkowski AV, Mebane LM, Philippar U, Barzik M, Rubinson DA, Gupton S, Van Veen JE, Furman C, Zhang J, *et al.* (2007). Filopodia are required for cortical neurite initiation. Nat Cell Biol 9, 1347–1359.

Desmarais V, Yamaguchi H, Oser M, Soon L, Mouneimne G, Sarmiento C, Eddy R, Condeelis J (2009). N-WASP and cortactin are involved in

invadopodium-dependent chemotaxis to EGF in breast tumor cells. Cell Motil Cytoskel 66, 303–316.
Di Ciano C, Nie Z, Szaszi K, Lewis A, Uruno T, Zhan X, Rotstein OD, Mak A, Kapus A (2002). Osmotic stress-induced remodeling of the cortical cytoskeleton. Am J Physiol Cell Physiol 283, C850–865.
Dickson BJ (2002). Molecular mechanisms of axon guidance. Science 298, 1959–1964.
Evans JV, Ammer AG, Jett JE, Bolcato CA, Breaux JC, Martin KH, Culp MV, Gannett PM, Weed SA (2012). Src binds cortactin through an SH2 domain cystine-mediated linkage. J Cell Sci 125, 6185–6197.
Faix J, Rottner K (2006). The making of filopodia. Curr Opin Cell Biol 18, 18–25.
Fan L, Di Ciano-Oliveira C, Weed SA, Craig AW, Greer PA, Rotstein OD, Kapus A (2004). Actin depolymerization-induced tyrosine phosphorylation of cortactin: the role of Fer kinase. Biochem J 380, 581–591.
Gallo G (2013). Mechanisms underlying the initiation and dynamics of neuronal filopodia: from neurite formation to synaptogenesis. Int Rev Cell Mol Biol 301, 95–156.
Gallo G, Lefcort FB, Letourneau PC (1997). The trkA receptor mediates growth cone turning toward a localized source of nerve growth factor. J Neurosci 17, 5445–5454.
Gomez TM, Letourneau PC (1994). Filopodia initiate choices made by sensory neuron growth cones at laminin/fibronectin borders in vitro. J Neurosci 14, 5959–5972.
Gomez TM, Letourneau PC (2014). Actin dynamics in growth cone motility and navigation. J Neurochem 129, 221–234.
Goncalves-Pimentel C, Gombos R, Mihaly J, Sanchez-Soriano N, Prokop A (2011). Dissecting regulatory networks of filopodia formation in a Drosophila growth cone model. PLoS One 6, e18340.
He Y, Ren Y, Wu B, Decourt B, Lee AC, Taylor A, Suter DM (2015). Src and cortactin promote lamellipodia protrusion and filopodia formation and stability in growth cones. Mol Biol Cell 26, 3229–3244.
Head JA, Jiang D, Li M, Zorn LJ, Schaefer EM, Parsons JT, Weed SA (2003). Cortactin tyrosine phosphorylation requires Rac1 activity and association with the cortical actin cytoskeleton. Mol Biol Cell 14, 3216–3229.
Heidemann SR, Lamoureux P, Buxbaum RE (1990). Growth cone behavior and production of traction force. J Cell Biol 111, 1949–1957.
Helgeson LA, Nolen BJ (2013). Mechanism of synergistic activation of Arp2/3 complex by cortactin and N-WASP. eLife 2, e00884.
Hoye AM, Couchman JR, Wewer UM, Yoneda A (2016). The phosphorylation and distribution of cortactin downstream of integrin alpha9beta1 affects cancer cell behaviour. Sci Rep 6, 28529.
Huang F, Hartwich TM, Rivera-Molina FE, Lin Y, Duim WC, Long JJ, Uchil PD, Myers JR, Baird MA, Mothes W, *et al.* (2013). Video-rate nanoscopy using sCMOS camera-specific single-molecule localization algorithms. Nat Methods 10, 653–658.
Huang C, Liu J, Haudenschild CC, Zhan X (1998). The role of tyrosine phosphorylation of cortactin in the locomotion of endothelial cells. J Biol Chem 273, 25770–25776.
Huang C, Ni Y, Wang T, Gao Y, Haudenschild CC, Zhan X (1997). Down-regulation of the filamentous actin cross-linking activity of cortactin by Src-mediated tyrosine phosphorylation. J Biol Chem 272, 13911–13915.
Kinley AW, Weed SA, Weaver AM, Karginov AV, Bissonette E, Cooper JA, Parsons JT (2003). Cortactin interacts with WIP in regulating Arp2/3 activation and membrane protrusion. Curr Biol 13, 384–393.
Knoll B, Drescher U (2004). Src family kinases are involved in EphA receptor-mediated retinal axon guidance. J Neurosci 24, 6248–6257.
Komano J, Miyauchi K, Matsuda Z, Yamamoto N (2004). Inhibiting the Arp2/3 complex limits infection of both intracellular mature vaccinia virus and primate lentiviruses. Mol Biol Cell 15, 5197–5207.
Korobova F, Svitkina T (2008). Arp2/3 complex is important for filopodia formation, growth cone motility, and neuritogenesis in neuronal cells. Mol Biol Cell 19, 1561–1574.
Kubo Y, Baba K, Toriyama M, Minegishi T, Sugiura T, Kozawa S, Ikeda K, Inagaki N (2015). Shootin1-cortactin interaction mediates signal-force transduction for axon outgrowth. J Cell Biol 210, 663–676.
Kurklinsky S, Chen J, McNiven MA (2011). Growth cone morphology and spreading are regulated by a dynamin-cortactin complex at point contacts in hippocampal neurons. J Neurochem 117, 48–60.
Lai FP, Szczodrak M, Oelkers JM, Ladwein M, Acconcia F, Benesch S, Auinger S, Faix J, Small JV, Polo S, *et al.* (2009). Cortactin promotes migration and platelet-derived growth factor-induced actin reorganization by signaling to Rho-GTPases. Mol Biol Cell 20, 3209–3223.
Lee AC, Decourt B, Suter D (2008). Neuronal cell cultures from aplysia for high-resolution imaging of growth cones. J Vis Exp 2008, 662.
Lewis AK, Bridgman PC (1992). Nerve growth cone lamellipodia contain two populations of actin filaments that differ in organization and polarity. J Cell Biol 119, 1219–1243.
Li W, Lee J, Vikis HG, Lee SH, Liu G, Aurandt J, Shen TL, Fearon ER, Guan JL, Han M, *et al.* (2004). Activation of FAK and Src are receptor-proximal events required for netrin signaling. Nat Neurosci 7, 1213–1221.
Lin CH, Espreafico EM, Mooseker MS, Forscher P (1996). Myosin drives retrograde F-actin flow in neuronal growth cones. Neuron 16, 769–782.
Liu G, Beggs H, Jurgensen C, Park HT, Tang H, Gorski J, Jones KR, Reichardt LF, Wu J, Rao Y (2004). Netrin requires focal adhesion kinase and Src family kinases for axon outgrowth and attraction. Nat Neurosci 7, 1222–1232.
Liu J, Huang C, Zhan X (1999). Src is required for cell migration and shape changes induced by fibroblast growth factor 1. Oncogene 18, 6700–6706.
Lowery LA, Van Vactor D (2009). The trip of the tip: understanding the growth cone machinery. Nat Rev Mol Cell Biol 10, 332–343.
Lua BL, Low BC (2005). Cortactin phosphorylation as a switch for actin cytoskeletal network and cell dynamics control. FEBS Lett 579, 577–585.
MacGrath SM, Koleske AJ (2012). Cortactin in cell migration and cancer at a glance. J Cell Sci 125, 1621–1626.
Magalhaes MA, Larson DR, Mader CC, Bravo-Cordero JJ, Gil-Henn H, Oser M, Chen X, Koleske AJ, Condeelis J (2011). Cortactin phosphorylation regulates cell invasion through a pH-dependent pathway. J Cell Biol 195, 903–920.
Mallavarapu A, Mitchison T (1999). Regulated actin cytoskeleton assembly at filopodium tips controls their extension and retraction. J Cell Biol 146, 1097–1106.
Martinez-Quiles N, Ho HY, Kirschner MW, Ramesh N, Geha RS (2004). Erk/Src phosphorylation of cortactin acts as a switch on-switch off mechanism that controls its ability to activate N-WASP. Mol Cell Biol 24, 5269–5280.
Martinez-Quiles N, Rohatgi R, Anton IM, Medina M, Saville SP, Miki H, Yamaguchi H, Takenawa T, Hartwig JH, Geha RS, Ramesh N (2001). WIP regulates N-WASP-mediated actin polymerization and filopodium formation. Nat Cell Biol 3, 484–491.
McConnell RE, Edward van Veen J, Vidaki M, Kwiatkowski AV, Meyer AS, Gertler FB (2016). A requirement for filopodia extension toward Slit during Robo-mediated axon repulsion. J Cell Biol 213, 261–274.
Mellor H (2010). The role of formins in filopodia formation. Biochim Biophys Acta 1803, 191–200.
Mezi S, Todi L, Orsi E, Angeloni A, Mancini P (2012). Involvement of the Src-cortactin pathway in migration induced by IGF-1 and EGF in human breast cancer cells. Int J Oncol 41, 2128–2138.
Navratil AM, Dozier MG, Whitesell JD, Clay CM, Roberson MS (2014). Role of cortactin in dynamic actin remodeling events in gonadotrope cells. Endocrinology 155, 548–557.
Nieto-Pelegrin E, Martinez-Quiles N (2009). Distinct phosphorylation requirements regulate cortactin activation by TirEPEC and its binding to N-WASP. Cell Comm Signal 7, 11.
Norris AD, Dyer JO, Lundquist EA (2009). The Arp2/3 complex, UNC-115/abLIM, and UNC-34/Enabled regulate axon guidance and growth cone filopodia formation in Caenorhabditis elegans. Neural Dev 4, 38.
O'Connor TP, Bentley D (1993). Accumulation of actin in subsets of pioneer growth cone filopodia in response to neural and epithelial guidance cues in situ. J Cell Biol 123, 935–948.
Olazabal IM, Machesky LM (2001). Abp1p and cortactin, new "hand-holds" for actin. J Cell Biol 154, 679–682.
Omotade OF, Pollitt SL, Zheng JQ (2017). Actin-based growth cone motility and guidance. Mol Cell Neurosci 84, 4–10.
Oser M, Mader CC, Gil-Henn H, Magalhaes M, Bravo-Cordero JJ, Koleske AJ, Condeelis J (2010). Specific tyrosine phosphorylation sites on cortactin regulate Nck1-dependent actin polymerization in invadopodia. J Cell Sci 123, 3662–3673.
Oser M, Yamaguchi H, Mader CC, Bravo-Cordero JJ, Arias M, Chen X, Desmarais V, van Rheenen J, Koleske AJ, Condeelis J (2009). Cortactin regulates cofilin and N-WASp activities to control the stages of invadopodium assembly and maturation. J Cell Biol 186, 571–587.
Ozcan AS (2017). Filopodia: a rapid structural plasticity substrate for fast learning. Front Synaptic Neurosci 9, 12.
Parsons SJ, Parsons JT (2004). Src family kinases, key regulators of signal transduction. Oncogene 23, 7906–7909.
Prager-Khoutorsky M, Spira ME (2009). Neurite retraction and regrowth regulated by membrane retrieval, membrane supply, and actin dynamics. Brain Res 1251, 65–79.

Radhakrishnan VM, Kojs P, Young G, Ramalingam R, Jagadish B, Mash EA, Martinez JD, Ghishan FK, Kiela PR (2014). pTyr421 cortactin is overexpressed in colon cancer and is dephosphorylated by curcumin: involvement of non-receptor type 1 protein tyrosine phosphatase (PTPN1). PLoS One 9, e85796.

Ren XL, Qiao YD, Li JY, Li XM, Zhang D, Zhang XJ, Zhu XH, Zhou WJ, Shi J, Wang W, *et al*. (2018). Cortactin recruits FMNL2 to promote actin polymerization and endosome motility in invadopodia formation. Cancer Lett 419, 245–256.

Robles E, Woo S, Gomez TM (2005). Src-dependent tyrosine phosphorylation at the tips of growth cone filopodia promotes extension. J Neurosci 25, 7669–7681.

Rosenberg BJ, Gil-Henn H, Mader CC, Halo T, Yin T, Condeelis J, Machida K, Wu YI, Koleske AJ (2017). Phosphorylated cortactin recruits Vav2 guanine nucleotide exchange factor to activate Rac3 and promote invadopodial function in invasive breast cancer cells. Mol Biol Cell 28, 1347–1360.

Roskoski R Jr (2004). Src protein-tyrosine kinase structure and regulation. Biochem Biophys Res Comm 324, 1155–1164.

Sanyal A, Chen AJ, Nakayasu ES, Lazar CS, Zbornik EA, Worby CA, Koller A, Mattoo S (2015). A novel link between Fic (filamentation induced by cAMP)-mediated adenylylation/AMPylation and the unfolded protein response. J Biol Chem 290, 8482–8499.

Schaefer AW, Kabir N, Forscher P (2002). Filopodia and actin arcs guide the assembly and transport of two populations of microtubules with unique dynamic parameters in neuronal growth cones. J Cell Biol 158, 139–152.

Schnoor M, Stradal TE, Rottner K (2018). Cortactin: cell functions of a multifaceted actin-binding protein. Trends Cell Biol 28, 79–98.

Siton O, Ideses Y, Albeck S, Unger T, Bershadsky AD, Gov NS, Bernheim-Groswasser A (2011). Cortactin releases the brakes in actin- based motility by enhancing WASP-VCA detachment from Arp2/3 branches. Curr Biol 21, 2092–2097.

Small JV, Stradal T, Vignal E, Rottner K (2002). The lamellipodium: where motility begins. Trends Cell Biol 12, 112–120.

Smith CL (1994). The initiation of neurite outgrowth by sympathetic neurons grown in vitro does not depend on assembly of microtubules. J Cell Biol 127, 1407–1418.

Spillane M, Ketschek A, Jones SL, Korobova F, Marsick B, Lanier L, Svitkina T, Gallo G (2011). The actin nucleating Arp2/3 complex contributes to the formation of axonal filopodia and branches through the regulation of actin patch precursors to filopodia. Dev Neurobiol 71, 747–758.

Strasser GA, Rahim NA, VanderWaal KE, Gertler FB, Lanier LM (2004). Arp2/3 is a negative regulator of growth cone translocation. Neuron 43, 81–94.

Suter DM, Forscher P (2000). Substrate-cytoskeletal coupling as a mechanism for the regulation of growth cone motility and guidance. J Neurobiol 44, 97–113.

Suter DM, Forscher P (2001). Transmission of growth cone traction force through apCAM-cytoskeletal linkages is regulated by Src family tyrosine kinase activity. J Cell Biol 155, 427–438.

Suter DM, Miller KE (2011). The emerging role of forces in axonal elongation. Prog Neurobiol 94, 91–101.

Svitkina TM, Bulanova EA, Chaga OY, Vignjevic DM, Kojima S, Vasiliev JM, Borisy GG (2003). Mechanism of filopodia initiation by reorganization of a dendritic network. J Cell Biol 160, 409–421.

Tagliabracci VS, Engel JL, Wen J, Wiley SE, Worby CA, Kinch LN, Xiao J, Grishin NV, Dixon JE (2012). Secreted kinase phosphorylates extracellular proteins that regulate biomineralization. Science 336, 1150–1153.

Tehrani S, Tomasevic N, Weed S, Sakowicz R, Cooper JA (2007). Src phosphorylation of cortactin enhances actin assembly. Proc Natl Acad Sci USA 104, 11933–11938.

Tokunaga M, Imamoto N, Sakata-Sogawa K (2008). Highly inclined thin illumination enables clear single-molecule imaging in cells. Nat Methods 5, 159–161.

Uruno T, Liu J, Zhang P, Fan Y, Egile C, Li R, Mueller SC, Zhan X (2001). Activation of Arp2/3 complex-mediated actin polymerization by cortactin. Nat Cell Biol 3, 259–266.

van Damme H, Brok H, Schuuring-Scholtes E, Schuuring E (1997). The redistribution of cortactin into cell-matrix contact sites in human carcinoma cells with 11q13 amplification is associated with both overexpression and post-translational modification. J Biol Chem 272, 7374–7380.

Vitriol EA, Zheng JQ (2012). Growth cone travel in space and time: the cellular ensemble of cytoskeleton, adhesion, and membrane. Neuron 73, 1068–1081.

Weaver AM, Karginov AV, Kinley AW, Weed SA, Li Y, Parsons JT, Cooper JA (2001). Cortactin promotes and stabilizes Arp2/3-induced actin filament network formation. Curr Biol 11, 370–374.

Weed SA, Karginov AV, Schafer DA, Weaver AM, Kinley AW, Cooper JA, Parsons JT (2000). Cortactin localization to sites of actin assembly in lamellipodia requires interactions with F-actin and the Arp2/3 complex. J Cell Biol 151, 29–40.

Weed SA, Parsons JT (2001). Cortactin: coupling membrane dynamics to cortical actin assembly. Oncogene 20, 6418–6434.

Weidmann MD, Surve CR, Eddy RJ, Chen X, Gertler FB, Sharma VP, Condeelis JS (2016). Mena(INV) dysregulates cortactin phosphorylation to promote invadopodium maturation. Sci Rep 6, 36142.

Wu B, Decourt B, Zabidi MA, Wuethrich LT, Kim WH, Zhou Z, MacIsaac K, Suter DM (2008). Microtubule-mediated Src tyrosine kinase trafficking in neuronal growth cones. Mol Biol Cell 19, 4611–4627.

Wu H, Parsons JT (1993). Cortactin, an 80/85-kilodalton pp60src substrate, is a filamentous actin-binding protein enriched in the cell cortex. J Cell Biol 120, 1417–1426.

Yamada H, Abe T, Satoh A, Okazaki N, Tago S, Kobayashi K, Yoshida Y, Oda Y, Watanabe M, Tomizawa K, *et al*. (2013). Stabilization of actin bundles by a dynamin 1/cortactin ring complex is necessary for growth cone filopodia. J Neurosci 33, 4514–4526.

Zhang ZY, Clemens JC, Schubert HL, Stuckey JA, Fischer MW, Hume DM, Saper MA, Dixon JE (1992). Expression, purification, and physicochemical characterization of a recombinant Yersinia protein tyrosine phosphatase. J Biol Chem 267, 23759–23766.

Zhang X, Yuan Z, Zhang Y, Yong S, Salas-Burgos A, Koomen J, Olashaw N, Parsons JT, Yang XJ, Dent SR, *et al*. (2007). HDAC6 modulates cell motility by altering the acetylation level of cortactin. Mol Cell 27, 197–213.

Zhu J, Yu D, Zeng XC, Zhou K, Zhan X (2007). Receptor-mediated endocytosis involves tyrosine phosphorylation of cortactin. J Biol Chem 282, 16086–16094.